frontiers | Frontiers in Nuclear Engineering

TYPE Review
PUBLISHED 07 February 2024
DOI 10.3389/fnuen.2024.1339222

OPEN ACCESS

EDITED BY
Anne Campbell,
Oak Ridge National Laboratory (DOE),
United States

REVIEWED BY
Jacob G. Fantidis,
International Hellenic University, Greece
Karim Ahmed,
Texas A and M University, United States
Stuart Maloy,
Pacific Northwest National Laboratory (DOE),
United States

*CORRESPONDENCE
Susan Ortner,
susan.r.ortner@uknnl.com

RECEIVED 15 November 2023
ACCEPTED 08 January 2024
PUBLISHED 07 February 2024

CITATION
Ortner S, Styman P and Long E (2024), The effects of flux on the radiation-induced embrittlement of reactor pressure vessel steels: review of current understanding and application to high fluences.
Front. Nucl. Eng. 3:1339222.
doi: 10.3389/fnuen.2024.1339222

The effects of flux on the radiation-induced embrittlement of reactor pressure vessel steels: review of current understanding and application to high fluences

Susan Ortner[1]*, Paul Styman[1] and Elliot Long[2]

[1]National Nuclear Laboratory, D5 Culham Science Centre, Abingdon, United Kingdom, [2]Materials Reliability Program (MRP), Electric Power Research Institute, Palo Alto, CA, United States

It is necessary to quantify the effects of flux on reactor pressure vessel steel embrittlement under neutron irradiation, if surveillance or high-flux test reactor data is used to predict vessel embrittlement occurring at lower fluxes. This is particularly important when considering embrittlement occurring during extended (60–80 years) operation for which there is no direct experience. Dedicated investigations are time-consuming and expensive even when only small flux-fluence ranges are investigated, so collating data from multiple campaigns is necessary to provide sufficient information to cover the wide range of fluxes required for vessel assessment in the long term. This paper collates and reviews such data. The review finds that flux dependences probably differ in sign and strength in different regimes (low flux and fluence, intermediate flux at low and high fluence, high flux at low and high fluence) with the regime limits affected by composition and temperature. The current understanding of diffusion processes and microstructural development are invaluable in interpreting the trends and limits. Many contradictory data sets were found, however, and not all contradictions could be dismissed as resulting from poor quality data. Suggestions are made for investigations to clarify the uncertainties. One wide-ranging model of flux effects, based on an extensive data set, is used to compare high-fluence data from different sources, to assess whether embrittlement rates accelerate after a high, threshold fluence. The model helps to identify experiments which investigated comparable flux-fluence-temperature regimes. The comparable data are split evenly between data sets supporting acceleration after a particular fluence and data sets contradicting it. The model identifies regimes in which further campaigns would clarify the causes of these contrasting observations.

KEYWORDS

flux, embrittlement, reactor pressure vessel, steel, radiation

1 Introduction

Extrapolating from currently-available data to predict reactor pressure vessel (RPV) condition during extended reactor lifetimes is viable only if the correct allowance is made for the dependence of RPV steel embrittlement on neutron flux. The aim of this review is, therefore, to collate and interpret the available data illustrating the effects of flux on steel

embrittlement, in support of predicting RPV condition assessment out to 60–80 years of operation. Mention will be made of modelling in support of data interpretation, but the focus of the review is on experimental data.

Although investigations into the effects of flux on embrittlement have been made over many decades, uncertainties remain, and these will be highlighted within the review to show where further work may help to resolve uncertainties and ambiguities. The uncertainties exist because the neutron fluxes relevant to RPV condition assessment cover an extremely wide range and the effect of flux may well vary within this range. For Boiling Water Reactors (BWRs), the neutron flux at the beltline inner wall is of the order 10^8–10^9 n.cm^{-2}s^{-11}, while for Pressurized Water Reactors (PWRs) it is around 10^{10}–10^{11} n.cm^{-2}s^{-1}. Through-wall attenuation reduces this by a factor of about 20 for PWRs, less for BWRs with their thinner walls. Information on changes in mechanical properties and microstructure under neutron irradiation comes primarily from surveillance programs and MTR campaigns. Surveillance specimens are generally irradiated at rates up to ×5 faster than the beltline inner wall, while MTR irradiations are, typically, at rates ×10 to ×10^4 more rapid than this. Understanding the relevance of MTR and surveillance data to degradation processes occurring within the RPV wall, thus requires trends in degradation with flux to be identified over many orders of magnitude.

Uncertainties and ambiguities also exist because investigating flux effects presents significant experimental challenges: achieving a meaningful fluence range over even one order of magnitude in flux requires a multiple-year campaign. Most campaigns must examine a small fluence range or compare a trend curve derived at one flux with individual measurements acquired at another, e.g., a trend derived from MTR data is compared with surveillance measurements on a similar material, or MTR measurements are compared with an embrittlement trend curve derived from analysis of a surveillance data base. Some, more extensive campaigns proceed in a stepwise fashion, with data acquired at pairs of low fluxes compared at low fluences and higher flux data compared over increasingly higher fluence ranges. The degree of overlap between steps is balanced between limiting the size of the campaign and limiting the range of fluxes examined. Comparing the results of different campaigns is vital to achieve a broad view and extract trends from scattered data. This paper provides an extensive review, collating data from multiple sources and both large and small campaigns.

The practical constraints on experimental investigations are compounded by the existence of multiple microstructural features capable of contributing to embrittlement and the non-monotonic relation between flux and the rate at which a given feature develops. A mechanistic framework derived from data interpretation and modelling is necessary to define flux/fluence/temperature/composition regimes within which particular processes may dominate and, hence, consistent trends may be observed. This review therefore separates the data based on the different microstructural components leading to embrittlement and the different flux-temperature regimes affecting the mobile point defect concentration or diffusion rate. The combination of the range of data sources and the organisation of the data within the review is intended to provide the clearest possible view of RPV steel behaviour.

1.1 Data organisation within the review

The specific definitions of the components used in this review are:

- Matrix defects or features (MDs or MFs are defined here as individual point defects and clusters of point defects and solute atoms in which the point defect concentration dominates. This includes vacancy or self-interstitial atom clusters, voids and dislocation loops).
- Solute clusters (SCs are clusters of point defects and solute atoms in which the solute content dominates, and which do not correspond to a phase with a lattice structure differing from that of the solid solution).
- Precipitates (These are solute dominated features which are energetically favoured based on the equilibrium or metastable phase diagram for the bulk steel composition or the composition in a local solute-enriched region of the irradiated steel. The equilibrium precipitates significant in MnMoNi RPV steels involve Cu and combinations of Ni, Si and Mn. Depending on the analysis technique used it is not easy to determine whether a solute-rich feature is a SC or a precipitate).
- Grain boundary segregants (Of greatest interest here are the desegregation of C and the segregation of P).

This leads to the division of the data into sub-sets based on steel composition and fluence: bulk Cu levels high enough to induce precipitation (high Cu); local or bulk Ni levels high enough to induce precipitation (high fluence or high Ni); conditions without identifiable precipitates (low Cu, low-moderate Ni and low-moderate fluence).

The different flux-temperature regimes considered here are those proposed originally by Sizmann (1978). The precise locations of the different regimes (in terms of flux, temperature, fluence and composition) are not known, and other regimes have been proposed. Nonetheless, Sizman's description provides a useful starting point, and one aim of the review is to determine whether sufficient data exist to locate the boundaries between the different regimes. Quantitative flux dependences in the different regimes were derived in Sizmann (1978) and are reported below for illustrative purposes, but have not been definitively confirmed.

- The thermal regime (At high temperatures and low fluxes, the radiation-induced defect concentration does not differ markedly from the equilibrium vacancy concentration, so thermal processes dominate. In this *thermal regime*, the diffusion rate is flux-independent, so any diffusion-controlled process is simply time-dependent. Expressing processes in terms of fluence then requires an inverse dependence on flux (damage proportional to $1/\phi$, where ϕ = flux).

1 Note that all fluxes and fluences are given in units of neutrons with energies >1 MeV unless otherwise stated.

- The fixed sink regime (With reducing temperatures and increasing dose rates, the radiation-induced defects begin to dominate. At intermediate temperatures, the point defects remain capable of rapid diffusion so, at low-to-moderate dose rates, they are likely to encounter a microstructural feature such as a dislocation or interface before annihilating with another point defect. In this regime, therefore, defects annihilate primarily at such fixed sinks. Attractions between point defects and the main solutes in RPV steels mean that the flux of defects drags solutes to or away from the sinks. In the *fixed sink regime*, the diffusion coefficient is proportional to ϕ^1, so the mean diffusion distance (a good correlate for the progress of a diffusion-controlled process) is independent of flux).
- The matrix recombination regime (At higher dose rates and lower temperatures still, the diffusion rates decrease, and the point defect concentrations rise until point defects can interact with each other after only short diffusion distances. This is the *recombination-dominated regime* (or *matrix recombination regime*). In this regime, solutes do not move over large distances via point defect interactions. In the matrix recombination regime, the diffusion coefficient is proportional to $\sqrt{\phi}$, so the progress of a microstructural change versus fluence is proportional to $1/\sqrt{\phi}$, becoming slower, with respect to fluence, at higher fluxes).

Around half the point defects produced initially will cluster within the cascade (i.e., at times < 50 ps) (Stoller, 2020), and cluster numbers increase with increasing dose (Stoller et al., 2003; Soneda, 2007). These clusters become progressively more important as sinks with increasing dose, reducing the rate of increase of mobile point defects with increasing flux and effectively expanding the fixed sink regime as the fluence increases. (Stoller et al., 2003; Odette et al., 2005; Soneda, 2007; Williams et al., 2010; Becquart and Wirth, 2020; Castin et al., 2020; Stoller, 2020).

Based on these descriptions, it is worth further dividing the data into sub-sets based on low, medium and high fluxes. With any choice of specific flux ranges, individual campaigns will often cover more than one range, so overlapping ranges have been chosen: low = surveillance ($<\sim10^{11}$ n.cm^{-2}s^{-1}), medium = MTR ($\sim10^{10}$–10^{12} n.cm^{-2}s^{-1}), high = accelerated MTR ($>\sim5 \times 10^{11}$ n.cm^{-2}s^{-1}).

2 Review of data on flux effects in low-Cu steels

In steels containing low levels of Cu, the hardening and embrittlement caused by irradiation to low-moderate fluences will be dominated by the formation of matrix defects. If point defect clustering is dominated by processes occurring in cascades, then matrix damage is expected to be independent of flux; if, however, longer-range diffusion processes cause significant changes to the post-cascade structures, then flux effects should be observed. Distinguishing between these alternatives is difficult because hardening increments in low-Cu steels tend to be small. Despite this difficulty, the low-Cu steels are considered first as the reduced number of contributors to embrittlement simplify the interpretation of the available data.

2.1 Low fluxes (low-moderate fluences)

Information concerning embrittlement at low fluxes comes from surveillance programs. These are not designed to provide single-variable comparisons, so extracting the flux contribution is hampered by effects of concurrently changing variables: there is a strong correlation between flux and fluence in any surveillance database; when the low-flux data are provided by BWR surveillance schemes and the high flux data by PWR schemes any other differences between BWRs and PWRs (chiefly operating temperature) correlate with flux. Nonetheless, it is worth noting that,

- Of the analyses of the US surveillance database (in which around one sixth of the data come from BWRs), most have not derived a flux-dependence for the matrix damage term but
  - o The 1998 analysis by Eason et al. (1998) contains a flux dependence in the matrix damage (Cu-independent) term,
  - o The 2001 analysis by Server et al. (2001) contains a flux dependence for matrix damage,
  - o The 2007 analysis by Eason et al. contains a flux dependence only below 4.4×10^{10} n.cm^{-2}s^{-1} (Eason et al., 2007), although it is not very strongly supported by the BWR data (EPRI, 2009).
- The French reactor fleet contains only PWRs and the French embrittlement trend curves (FIS and FIM) contain no flux dependence in the matrix damage term.
- The Belgian embrittlement trend curve (RADAMO) contains no flux term (Chaouadi, 2005).
- The embrittlement trend curve (ETC) in the ASTM E900-15 standard (ASTM, 2015) is derived from a database dominated by US data but containing a significant amount of data from other countries. Around one sixth of the data comes from BWRs and the ETC does not contain a flux term in the Cu-independent term.
- The Japanese JEAC4201 ETCs are based on surveillance data derived from a fleet which contains similar numbers of BWRs and PWRs, and the ETCs include a flux term for matrix damage (Tomimatsu et al., 1994; Soneda and Nomoto, 2008; Hashimoto et al., 2021).

On this basis, it is plausible that the thermal regime appears within the range of BWR surveillance data (at fluxes of the order 10^{10} n.cm^{-2}s^{-1}) with the fixed sink regime at higher fluxes, and that this affects matrix damage development.

It should be noted, however, that the temperature dependence in the Japanese ETCs tends to be weaker than in other ETCs, so some conflating of flux and temperature effects may be occurring. A dedicated analysis of international surveillance data with the aim of identifying whether a low-flux regime of flux-dependence is appearing would be useful.

2 Reprinted from J. Nuclear Mater., Vol 418, Chaouadi, R.; Gerard, R., Neutron flux and annealing effects on irradiation hardening of RPV materials, Pages 137–142, Copyright (2011), with permission from Elsevier.

2.2 Intermediate fluxes (low-moderate fluences)

Experimental investigations at higher fluxes are dominated by the large campaigns led by the UCSB group of G. R. Odette. Few other programs have been as extensive or as well-controlled, to minimize ambiguity from concurrently changing variables. The results from the UCSB campaigns will, therefore, be presented first, and data from other campaigns (whether conducted earlier or later) will be presented in the context of the UCSB work.

2.2.1 UCSB campaigns

In their IVAR (Irradiation Variables) program, the UCSB group investigated a flux range which overlaps with the range of PWR surveillance fluxes but reaches to higher fluxes (nominally 8×10^{10}, 3×10^{11} and 8×10^{11} n.cm^{-2}s^{-1}). Steels with a wide range of compositions (Cu = 0–0.43, Ni = 0–1.7, Mn = 0–1.7, P = 0.002–0.035 wt%) were irradiated at a range of temperatures (270, 290, and 310°C) to fluences up to 4×10^{18} n.cm^{-2} (low flux) – 3×10^{19} n.cm^{-2} (high flux). Portions of the data are reported and analyzed in multiple publications, but the full set is provided in association with (Eason et al., 2007), where the data trends are discussed in detail.

Of the ten low-Cu (<0.08 wt%), medium-Ni (<1 wt%) and two low-Cu, high-Ni (1.6–1.7 wt%) steels examined in the IVAR campaign, eight showed clear trends with flux in the residuals when the measured hardening was compared with a (flux-independent) trend curve developed for surveillance data by Eason et al. (2007) (four showed negligible trends; none showed a positive trend). This led Odette and co-workers to conclude that there was a small but consistent flux-dependence to stable matrix damage (SMD) in this flux/fluence/temperature range. They incorporated this into a flux-compensated "effective fluence" defined by:

$$Effective\ fluence = \varphi t_e = \varphi t\left(\frac{\varphi_r}{\varphi}\right)^p \quad (1)$$

Equation 1: Odette et al.'s definition of effective fluence
where ϕ_r = reference flux, here 3×10^{11} n.cm^{-2}s^{-1}
p = constant fitted to each composition (=0.42–0.47)

Note that this indicates that increasing the flux delays microstructural development to higher fluences, partly offsetting the advantage of using higher fluxes to identify high-fluence behaviour. An associated rate theory model interpreting this trend was presented in (Odette et al., 2005), but will not be assessed within this review, which is focused on the accumulation of support for particular trends.

2.2.2 Other campaigns

The flux-dependence in the IVAR data was confirmed by other authors and methods (Williams et al., 2010; Mathew et al., 2018). The flux dependence has, however, been difficult to reproduce in other data sets. In the most closely comparable campaign, Dohi et al. (2001) obtained both tensile and Charpy data from two different low-Cu, medium-Ni base metals after irradiation at 3 (tensile) or 4 (Charpy) different fluxes to 10^{18} n.cm^{-2} and after 2 and 3 fluxes at 10^{19} n.cm^{-2}. The fluxes at 10^{18} n.cm^{-2} overlap the IVAR range very closely, but the authors did not find any trend in their data within scatter. Other authors who examined low-Cu material within the IVAR range have fewer materials or measurements (Bourgoin et al., 2001; Wagner et al., 2016), so the absences of flux effects in their individual observations carry less weight. Nonetheless, the accumulation of campaigns in which the IVAR trend was not reproduced is a matter for concern, and confirmation from datasets from other sources would be desirable.

2.2.3 Implications

The immediate importance of the trend in matrix damage seen in the IVAR data was that, if continued to lower fluxes, it would cause higher-flux data to underestimate the hardening rate at lower fluxes. Artificial neural network analysis of IVAR and US LWR surveillance data (a set with very few data below 10^{10} n.cm^{-2}s^{-1}) (Mathew et al., 2018) used a consistent methodology to confirm that the flux dependence was indeed significant within the IVAR data set but not within the (PWR) surveillance set, suggesting that p (Eq. 1) drops to zero below about 10^{11} n.cm^{-2}s^{-1}. Comparing this outcome with the earlier assessment of surveillance data suggests that the fixed sink regime covers the range 10^{10}–10^{11} n.cm^{-2}s^{-1}, with the thermal regime probably intervening at lower fluxes.

Based on the combined observations, the PWR beltline inner wall can be described by surveillance data without a flux correction. Whether through-wall attenuation effects require a flux correction, and whether the state of the BWR beltline inner wall is correctly assessed with a flux-independent trend curve derived from predominantly PWR data, remain unclear from these low-Cu steel data. Given the magnitudes of the effects observed, however, differences between BWR surveillance samples and the BWR inner wall (a ×3 to ×5 change in flux) will be very small, even if one or both lie within the thermal regime.

2.3 High fluxes (low and high fluences)

2.3.1 UCSB and RADAMO campaigns

In the 1990s Odette and co-workers exposed A533B-type steels of multiple compositions at high fluxes 5×10^{11}–6×10^{13} n.cm^{-2}s^{-1}, in the University of Virginia and PLUTO MTRs (the UV-P campaign) (Odette et al., 1993; Mader, 1995). They found that hardening at a given fluence in 0.4 wt% Cu steels decreased with increasing flux while that in 0.11–0.16 wt% Cu steels increased. They interpreted this as indicating that two opposing flux dependences existed, one in MDs and the other in Cu-rich SCs. This MD contribution added increasingly to hardening at fluxes above 4×10^{12} n.cm^{-2}s^{-1}. Data (Mader, 1995) from steels with <~0.01 wt% Cu confirmed that the appropriate trend occurred when only matrix damage was present, as illustrated in Figure 1.

It is important to note that (1) the hardening increments shown are small (15–35 Vickers hardness points) and comparable with measurement uncertainty, even though great care was taken to minimize the uncertainties, and (2) the fluences involved are small.

3 Reprinted from Nuclear Engineering and Design., Vol 273, Kryukov, A.; Nanstad, R. K.; Brumovsky, M. Common comparison of the irradiation embrittlement of WWER/PWR reactor pressure vessel steels, Pages 175–180, Copyright (2014), with permission from Elsevier.

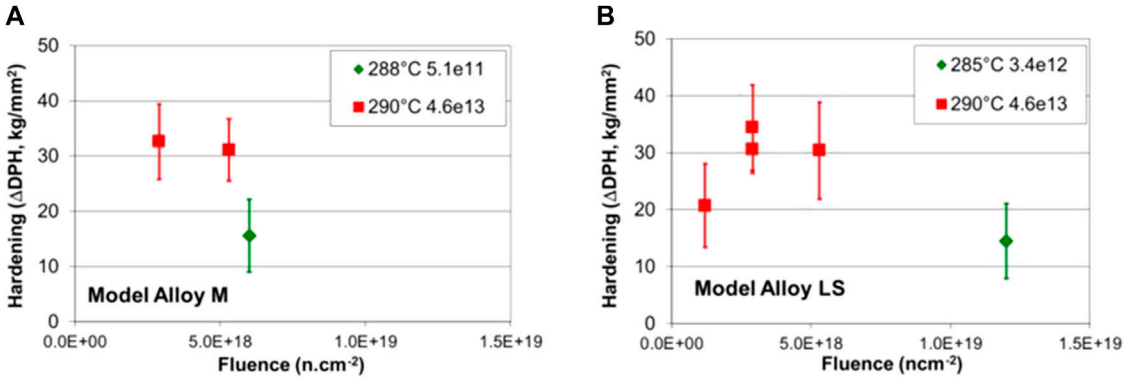

FIGURE 1
Effect of flux on hardening in UV-P campaign **(A)** 0.01Cu 0.6Ni Model Alloy M in temperature range 288°C–290°C **(B)** 0.005Cu 0.74Ni Model Alloy LS in temperature range 285°C–290°C [data from (Mader, 1995)].

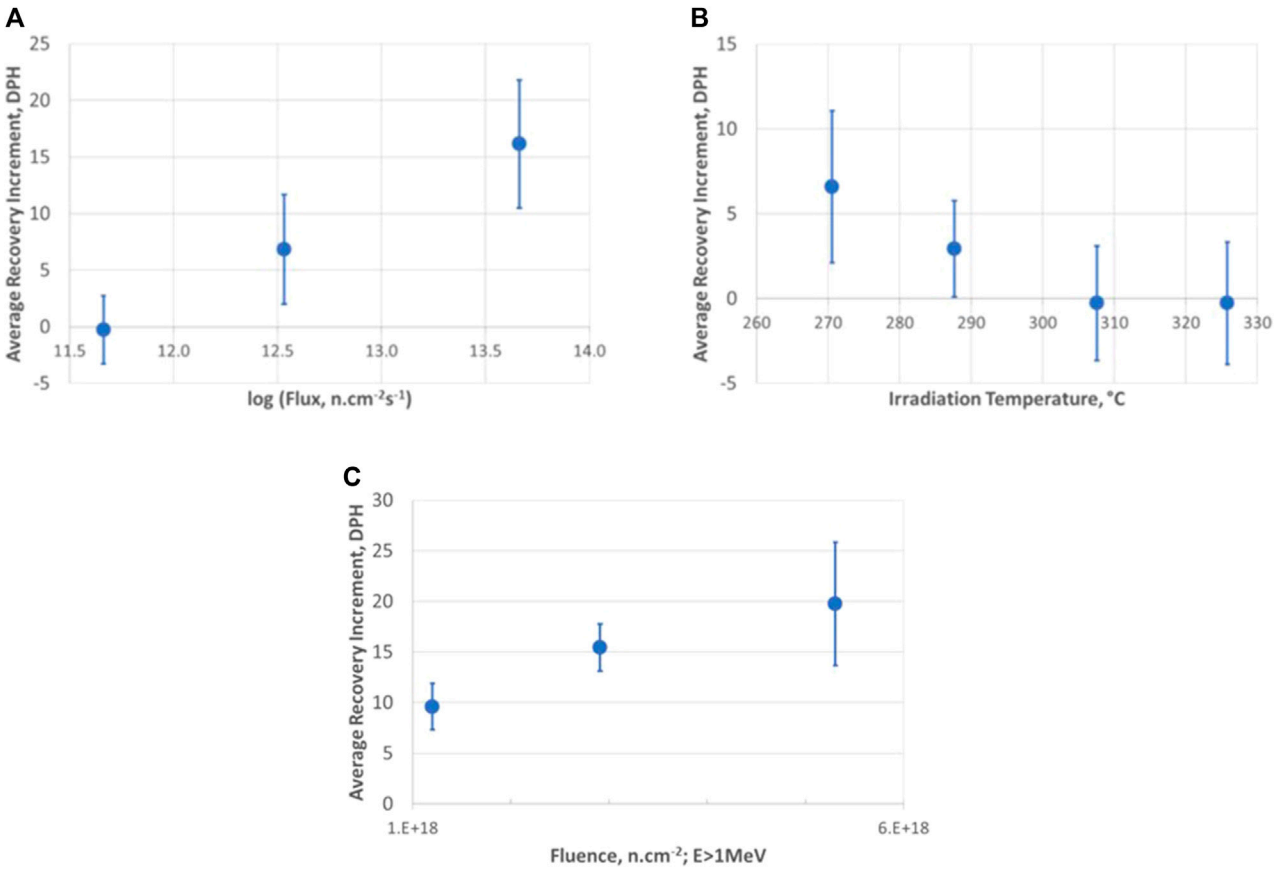

FIGURE 2
Hardness recovered during low temperature (150 h 290°C or 5 h 343°C) annealing of an RPV steel as a function of **(A)** flux (after irradiation to 6 × 10^{19}n.cm^{-2} at 290°C) **(B)** irradiation temperature (after irradiation to 10^{19}n.cm^{-2} at 4.5 × 10^{12}n.cm^{-2}s^{-1} **(C)** fluence (after irradiation at 290°C and 4.6 × 10^{13}n.cm^{-2}s^{-1}) (data from (Castin et al., 2011)).

Associated low-temperature post-irradiation annealing (PIA) indicated that measurable recovery occurred within 5 h 343°C after the higher-flux irradiations, as illustrated in Figure 1. The average recovery increments increase with increasing flux and fluence and decreasing temperature and are similar in magnitude to the additional high-flux hardening illustrated in Figure 1. Odette and co-workers interpreted this as showing that a population of matrix defects, unstable at the irradiation temperature ("Unstable Matrix Defects/Features", UMDs/UMFs) contributed increasingly to hardening at high fluxes. It should, however, be recognized that the PIA behavior could also have indicated an increasing contribution from matrix recombination with increasing flux. (In the fixed sink regime, vacancies and SIAs reach independent equilibria with the fixed sinks, so loss of hardening during PIA would reflect the contribution of only the unstable defects. In the matrix recombination regime, however, loss of unstable vacancy-type defects would involve annihilation with stable SIA defects and *vice versa*, so the loss of hardness during PIA would reflect the loss of both unstable and otherwise stable defects). In addition, the annealing increments displayed in Figure 2 appear to have been averaged over results from steels with Cu levels from 0–0.8 wt%, with the UMD contribution to hardening increasing with increasing Cu (Mader, 1995). This was originally considered to be justified as SANS indicated that the Cu-rich SCs were unaffected by the annealing treatment (Mader, 1995). In later APT analyses of low-temperature annealed steels, however, it appeared that a short annealing treatment does affect the SC population (Soneda, 2010), inducing softening. The average PIA increments in Figure 2 will, thus, be an upper limit to the UMD contribution to annealing, even as the PIA contribution itself is an upper limit to the defects' hardening contribution in low-Cu steels.

Overall, Odette and co-workers observed a consistent trend in the hardening and annealing of several Cu < 0.01 wt% steels in the UV-P campaign. The model they derived included flux dependences for both UMDs and SCs and reconciled the hardening and annealing behavior of multiple steels within this program. Nonetheless, these observations of UMD effects conflicted with the lack of a flux dependence seen in the tensile data in the extensive Belgian RADAMO database (Chaouadi, 2005; Castin et al., 2011; Chaouadi and Gerard, 2011; Chaouadi and Gerard, 2013).

The RADAMO database did not incorporate such a systematic variation in material compositions as the UCSB UV-P campaign but involved multiple steels with a range of compositions within RPV steel specifications. It was built up largely from irradiations in the BR2 MTR at 300°C and covered a similar flux range to the UV-P campaign, although the exposures were generally taken to higher fluences than in the UV-P campaign. The relatively high irradiation temperature would be predicted to reduce the UMD effect (Figure 2C), and there is some tendency for lower-fluence RADAMO data to have been acquired at lower fluxes. Given the small size and upper bound nature of the UMD increments shown in Figures 1, 2, this might be sufficient to account for the flux-independence seen in the RADAMO tensile data.

Another possible contributor to the contrasting observations made within the UCSB and RADAMO campaigns is the fluence range. The UV-P data were mostly acquired at $<10^{19}$ n.cm^{-2}, while the RADAMO data were mostly acquired in the range 0.5–10 × 10^{19} n.cm^{-2}. At the higher fluences, the presence of large numbers of stable matrix features (SMFs) might overwhelm the contribution of the UMDs.

In an effort to clarify the alternative views, Odette et al. irradiated one of the UCSB model steels (LG = 0Cu, 0.8Ni) in the BR2 reactor (Toyama et al., 2020). The hardening at fluences up to 2 × 10^{19} n.cm^{-2} was similar after the high-flux BR2 irradiations (1.4 × 10^{12} n.cm^{-2}s^{-1} or 10^{14} n.cm^{-2}s^{-1}) and IVAR campaigns (0.3 and 0.8 × 10^{12} n.cm^{-2}s^{-1}). The BR2 hardening, however, was almost entirely recovered during low-temperature annealing, while the IVAR samples showed no recovery. After 3.3 × 10^{19} n.cm^{-2}, the BR2 sample showed around 10Hv more hardening than the IVAR sample: the difference was recovered within PIA 5 h 343°C or during isochronal annealing in 20-min, 25°C-increments from 275°C–375°C. The UCSB group concluded that their BR2 campaign confirmed the existence of UMDs and their increasing contribution with increasing flux and fluence. Nonetheless, the difference in the fluence ranges over which UMD hardening increments were seen in the UV-P and IVAR-BR2 campaigns shows again the smallness of the systematic effect with respect to measurement uncertainties. Subsequent PIA of the RADAMO steels by SCK.CEN, found no reductions in hardness after low-temperature PIA of steels which the UCSB group would have predicted to show UMD annealing (Chaouadi and Gerard, 2013).

In their more recent, ATR campaigns (Odette et al., 2016), the UCSB group irradiated very low Cu steels in the range 10^{12}–10^{14} n.cm^{-2}s^{-1} to much higher fluences (from the mid-10^{19} to 10^{21} n.cm^{-2}). Solute clustering dominated by Mn, Ni and Si (possibly precipitation) was observed above 10^{20} n.cm^{-2} in a medium-Ni steel and at lower fluences in a high-Ni (1.6wt%) steel. Unlike in the UV-P and BR2 campaigns, the hardening after irradiation at 10^{14} n.cm^{-2}s^{-1} data in the ATR campaign was not evidently greater than that after 10^{11} and 10^{12} n.cm^{-2}s^{-1}, even at the lowest fluences shown (1-3 × 10^{19} n.cm^{-2}s^{-1} depending on the steel). If this is because the significance of a UMD component diminishes above about 10^{19} n.cm^{-2}, then this would reconcile the ATR and UV-P observations, but it does not clarify the BR2 observations.

At the high fluences above which Mn-Ni-Si clustering was seen, the UCSB group found that the hardening at different fluxes could, again, be made to converge via use of the effective fluence, though now with a smaller value of p (Eq. 1) than at the IVAR fluxes-fluences. The flux-dependence is weaker than in the IVAR data because of the larger number of sinks present at the high fluences of the ATR experiments.

In their most recent analysis of ATR2 data, Odette and co-workers (OWAY) have concluded that there is no net effect of flux in the range 6–14 × 10^{19} n.cm^{-2} and 3.7 × 10^{12}–10^{14} n.cm^{-2} (Nanstad et al., 2022). This is not immediately evident in the plots of (Odette et al., 2016). Possibly (i) the restriction in the flux-fluence range of the OWAY data makes any flux effect more difficult to extract from measurement uncertainty and/or (ii) the aspect of the OWAY analysis which postulates linear hardening versus log fluence in this fluence range affects the apparent contribution of flux.

Summarizing the various UCSB campaigns, the following trends in hardening in low-Cu steels were identified:

- Hardening decreases with increasing flux in the range 0.8–8 × 10^{11} n.cm^{-2}s^{-1} and 0.4–3 × 10^{19} n.cm^{-2} (SMF effect);
- Hardening increases with increasing flux in the range 0.4–46 × 10^{12} n.cm^{-2}s^{-1} and 1–8 × 10^{18} n.cm^{-2} (UMD effect);
- Hardening decreases with increasing flux in the range 10^{12}–10^{14} n.cm^{-2}s^{-1} and 0.5–12 × 10^{20} n.cm^{-2}, but less strongly than at lower fluxes (MNS effect at high fluences).

The UCSB campaigns thus predict that there are transitions in the direction of the flux effect around 10^{12} n.cm^{-2}s^{-1} at low fluences (SMF↔UMD) and around 5 × 10^{19} n.cm^{-2} at high fluxes (UMD↔MNS). In this context, it is possible that some of the RADAMO data may have been acquired over a fluence range between that dominated by UMDs (hardening increases with increasing flux) and that dominated by MNSs (hardening deceases with increasing flux). The contrasting PIA responses in the UCSB and RADAMO steels after BR2 irradiations, however, remain unexplained.

2.3.2 Other campaigns

The different flux dependences found by the UCSB group in each flux-fluence range examined make comparisons between UCSB and other data difficult. Few other campaigns compare hardening in low-Cu steels at different fluxes within only one of the flux-fluence ranges examined by the UCSB group, or to only one side of the transitions. Most studies tend to compare data from within or below the IVAR range with data from within the UV-P range (Petrequin, 1996; Xu et al., 2000; Langer et al., 2001; Yamamoto et al., 2001; Gerard et al., 2006; Hein and May, 2008; Soneda et al., 2008; Soneda et al., 2015; Wagner et al., 2016; Lindgren et al., 2017; Burke et al., 2003; Japan Nuclear Energy Safety Organisation, 2009; Soneda et al., 2009). Under these circumstances, it becomes impossible to distinguish between the presence of a changing flux dependence and the absence of any flux-dependence. In addition, the small sizes of the flux-dependent increments mean that large databases are required to identify the trends. Indeed, most of these groups interpret their data as showing no effect of flux.

A large database was investigated by Kirk and co-workers' analysis of the surveillance and MTR embrittlement data in the PLOTTER database [in (Kirk and Ferreno Blanco, 2022) and Appendix B of (Kirk and Erickson, 2021)]. The surveillance data had been used to derive the E900-15, ETC and were, in consequence, well-described by it without a flux-dependence in the low-Cu term. The MTR low-Cu data, however, showed a bias towards underprediction, interpretable as an increase in hardening with increasing flux. Such a bias would be consistent with the introduction of UMFs, but the fluence ranges involved are higher than that used in the UV-P campaign. In the relevant fluence range (between 10^{19} and 10^{20} n.cm^{-2}) the IVAR and ATR campaigns showed a decrease in hardening with increasing flux and the RADAMO campaign showed no effect of flux. One possible explanation for Kirk and co-workers' contrary observation is that it did not involve a focused, single-variable investigation, but a statistical analysis of data from multiple campaigns in multiple reactors/reactor locations. In some of the MTR irradiations within PLOTTER, the dpa levels associated with a particular fluence (E > 1 MeV) can vary by a factor of 2. The apparent flux effect in PLOTTER may, therefore, reflect the different dpa values in different campaigns. A dedicated analysis program would, however, be required to determine whether this is a significant contributory factor.

Another compilation of data was made by Williams and co-workers at Rolls-Royce (RR) in collaboration with UCSB. In the analysis of their own data on low-Ni and high-Ni submerged-arc welds (SAWs) Williams identified no effects of flux (Williams et al., 2001a; Williams et al., 2001b; Williams and Ellis, 2001). (See Figure 3.) They then added the IVAR data, US and French surveillance data, data from the IAEA Coordinated Research Program IAEA-CRP3, and data from Bettis Laboratory to their compilation, using dpa as the damage correlate to avoid the problem of differing neutron spectra. Considering only low-Cu (<0.075 wt%) materials irradiated at dose rates <=1.5 × 10^{-9} dpa/s (~10^{12} n.cm^{-2}s^{-1}), that is steels damaged by SMFs (Williams et al., 2010), they found hardening to decrease with increasing flux. Essentially, the trend in the IVAR data was supported (or at least not offset by) the additional data. No thermal regime was identified, consistent with previous analyses of the US and French surveillance databases.

Their overall analysis incorporated an effective fluence, $(\varphi t)_{eff} = Q(\varphi t)$: the flux and temperature dependences of Q are shown in Figure 4, (Williams et al., 2010). This describes a fixed sink (flux-independent) regime below 10^{-10}dpa/s at 320°C, decreasing with decreasing irradiation temperature, and a higher flux trend of decreasing hardening rates with increasing fluxes, intensified if UMDs exist.

Williams and co-workers used a combination of PIA (to isolate any UMD contribution), atom probe tomography (to isolate any Mn-Ni-Si clustering contribution), thermal ageing and modelling to assign increments to the different components and concluded that a UMD effect was introduced above 10^{12} n.cm^{-2}s^{-1} but saturated above 0.1 dpa (about 6 × 10^{19} n.cm^{-2}). A hardening increment due to Mn-Ni-Si-containing SCs (or precipitates) appeared above about 0.07 dpa (5 × 10^{19} n.cm^{-2}) in the high-Ni steels and increased with increasing dose. Since the UMDs could act as sinks for point defects, they were expected to reduce the rate at which SMFs and SCs develop. The presence of UMDs thus does not necessarily result in higher overall hardening at all fluences; under some conditions, it will merely redistribute a similar amount of hardening between different contributors.

The UMD contribution to hardening determined by Williams and co-workers is retained to a higher dose than the 10^{19} n.cm^{-2} limit which would have reconciled the UCSB UV-P and RADAMO data, but the irradiation temperature in the high-dose RR data is lower (255°C) than in the UV-P or RADAMO irradiations, and low temperatures were predicted to enhance the UMD effect (Mader, 1995; Odette and Lucas, 1998), so the difference may not be significant. Retention of a UMD effect up to 10^{20} n.cm^{-2} is, however, difficult to reconcile with the ATR data (Odette et al., 2016) (which show the opposite flux dependence in this fluence range even in the absence of MNS clusters) or the RADAMO data (showing no flux dependence). Saturation of the UMD effect around 6 × 10^{19} n.cm^{-2}, is also not consistent with the original analysis of the UCSB BR2 observations in which low-temperature PIA removed increasing amounts of hardening up to the maximum fluence of 1.2 × 10^{20} n.cm^{-2}.

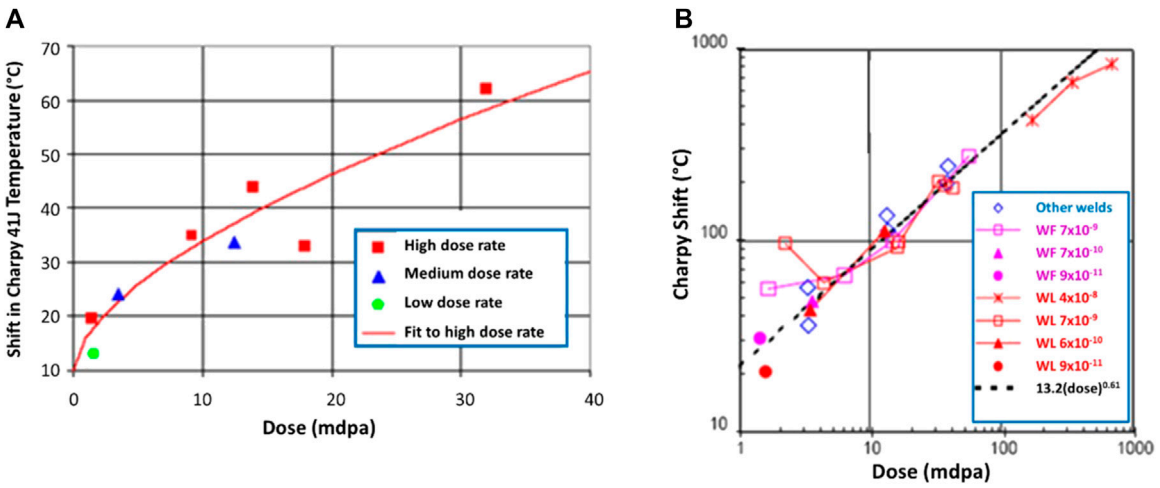

FIGURE 3
Williams and co-workers' hardening data from low-Cu SAWs, compared with trend curves without flux dependences **(A)** low-Ni SAWs, **(B)** high-Ni SAWs (Williams et al., 2001b; Williams and Ellis, 2001).

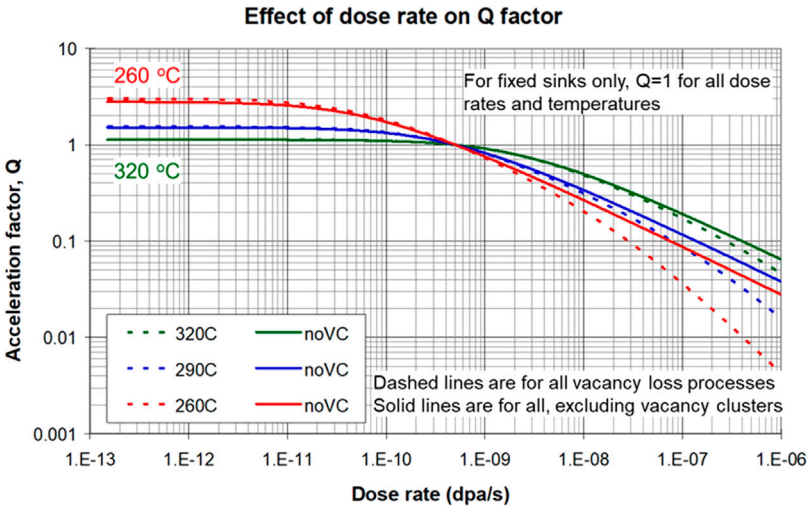

FIGURE 4
Flux-dependence of the fluence acceleration factor at different temperatures with and without a contribution from vacancy clusters (UMDs) from Williams and co-workers' data compilation (Williams et al., 2010).

2.3.3 Summary of flux effects seen in low-Cu steels and implications

A summary of the different studies on low-Cu steels is given in Figure 5. The numbers across the top indicate the log(flux), such that the bars indicate the range of fluxes in each investigation. If the data are found over multiple fluxes within the range, the bar is solid; if the data were acquired at specific, widely separated fluxes within the range, then the fluxes without data are shown hatched. If the authors found an increase in hardening/embrittlement with increasing flux over the flux range, the bar is red; if they found a decrease with increasing flux, the bar is blue; if no trend was observed, the bar is green. The final column shows the number of different materials involved in each campaign. Clearly a trend seen for multiple materials is more significant than when only one material is involved. The overlap in data (i.e., whether low-flux-and-fluence data are compared with extrapolations from trends drawn through high-fluxes-and-fluences or whether similar fluences are reached with different fluxes) is also important, but more difficult to quantify.

The plot makes it clear that the extensive, single-variable experimental campaigns set up by the UCSB group identified small, but consistently measurable effects of flux on hardening in low-Cu steels, with different trends in the flux-fluence range of each campaign. These trends are also seen in Williams et al.'s compilation including UCSB data, but data from other sources often fail to agree with the trends observed in the UCSB campaigns.

FIGURE 5
Summary of observations on low-Cu steels. Most observations were made at 270°C–310°C. Those marked with an asterisk (*) involved lower irradiation temperatures.

The different trends (or lack of trends) seen in different data sets cannot all be immediately ascribed to measurement uncertainty, even though the absolute values of shifts in low-Cu steels tend to be small. It is feasible that some properties not widely reported (e.g., C or N content, thermomechanical history) affect the transitions between different flux-fluence regimes, such that different materials exposed in a given flux-fluence range can be experiencing different mechanistic regimes. It is also feasible that neutron energy spectra affect comparisons between data acquired in different locations.

The main questions and knowledge gaps concerning low-Cu steels are, thus:

- Does a thermal regime affect hardening in low-Cu steels at BWR surveillance fluxes?
- What causes the contrasting trends observed by different groups in similar MTR flux-fluence ranges?
- Can a program of experiment, analysis/reanalysis, or modelling be defined which would reconcile the currently conflicting trends seen in different data sets (possibly including an updated analysis of dpa/fluence ratios in relevant reactor locations)?
- If UMFs are real, what is the range over which they affect hardening, since reconciliation between UV-P and RADAMO might indicate a limit of around 10^{19} n.cm^{-2}; while the RR/UCSB compilation and analysis of the PLOTTER database would suggest a limit around 10^{20} n.cm^{-2}.
  - o Does PIA really characterize a UMF contribution to hardening?

Settling these questions is technologically important because nuclear power plants with low-Cu RPV steels are those for which operators are most likely to apply for license to extend plant lifetimes. If there is no overall effect of flux, then an accelerated irradiation can directly identify the fluence at which a new hardening component appears, allowing operational behaviour to be predicted out to 80 or even 100 years. Allowing for flux dependences of different sign in different flux-fluence-temperature ranges means that no general statement can be made. Based on the various UCSB campaigns and the RR/UCSB compilation analysis, it appears that measurements made on steels irradiated to around 10^{20}n.cm^{-2} or above, after irradiations at 10^{12}–10^{14}n.cm^{-2}s^{-1} will underestimate the embrittlement of low-Cu steels after surveillance or

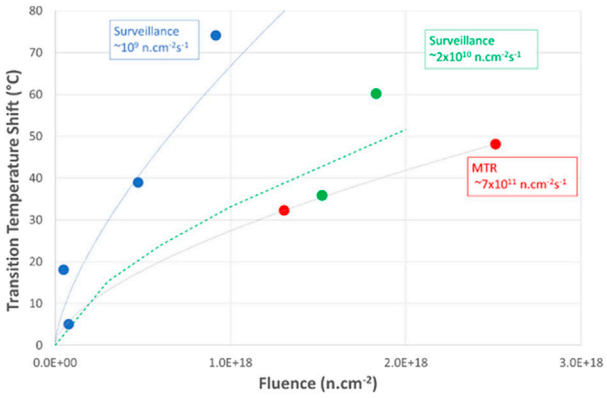

FIGURE 6
Effect of flux on embrittlement of 0.24Cu, 0.6Ni mod A302B base metal SP, irradiated at about 276°C (Data from (Soneda, 2007). Lines indicate best power law fits to data.).

operational exposures to a similar fluence. This is considered further in Section 5.1.

3 Review of data from high-Cu steels at low-moderate fluences

The beltlines of RPVs in modern NPP are not generally manufactured from high-Cu steels (steels with Cu levels >0.08 wt% for the purposes of this review). Nonetheless, information on flux or high-fluence effects in high-Cu steels is relevant to modern plant in that it can aid in the interpretation of otherwise ambiguous data from low-Cu steels. Unlike matrix defects, solute clusters are expected to grow predominantly via diffusion outside cascades. This makes the clustering/precipitation of Cu and other solutes more strongly diffusion dependent than MD formation. At the same time, the overall hardening in the presence of Cu is greater than in low-Cu steels, so trends with material and environmental parameters are easier to distinguish from measurement uncertainty.

More directly, components which were not considered as subject to radiation-induced degradation in current LWRs operating for 40 years may experience sufficient exposure to experience degradation during 60–80 years of operation. The composition control of such components will not have been as tight as that of beltline components, so some will contain high levels of Cu. Any low-flux flux dependences present in the embrittlement of high-Cu steels will affect the prediction of embrittlement in these components.

The behavior of Cu-containing steels is best understood if it is separated into the fluence ranges (1) during which Cu is precipitating and (2) after most of the Cu has precipitated and the Cu contribution to hardening has reached a maximum, or a constant value with further increases in fluence (the "plateau"). Fluences in the range below 10^{19} n.cm^{-2} are generally in the pre-plateau region, with the plateau onset around 1–2 × 10^{19} n.cm^{-2}, depending somewhat on material and irradiation variables.

3.1 Low-intermediate fluxes (<10^{12} n.cm^{-2}) and low fluences (pre-plateau)

As with MD terms, the copper clustering terms in most analyses of PWR-dominated surveillance data are independent of flux, but the Japanese JEAC4201 trend curve (derived from a BWR-dominated fleet) and the part of the EONY analysis of US LWR surveillance data applicable to BWR data both incorporate a flux-dependence for copper clustering (Brillaud and Hedin, 1992; Bourgoin et al., 2001). This supports the possibility that the onset of the thermal regime lies within, rather than below, the flux range of BWR surveillance data.

This interpretation of statistical trends in surveillance data is subject to the caveat that flux is readily conflated with fluence and temperature effects in the statistical analysis of surveillance data. More direct support for the location of the thermal regime is provided by the comparison between BWR surveillance data and higher-flux irradiations illustrated in Figure 6 (Soneda, 2007). The hardening at low fluences (pre-plateau hardening) in the high-Cu steel SP is clearly more rapid at the very low flux ("Surveillance W", ~10^{9} n.cm^{-2}s^{-1}) than at the low flux ("Surveillance A″, ~2 × 10^{10} n.cm^{-2}s^{-1}) or intermediate flux ("MTR", 7 × 10^{11} n.cm^{-2}s^{-1}). This is reflected in microstructural analyses which show the Cu coming out of solution more rapidly (with respect to fluence, not time) at the lower flux.

The change in flux between the higher surveillance and MTR exposures is somewhat greater (×35) than that between the two surveillance exposures (×20), but the change in embrittlement is greatest between the two surveillance fluxes in Figure 6. The rate of change of embrittlement with flux is, thus diminishing in this flux range. This would be consistent with a shift from a (more strongly flux-dependent) thermal regime to a (flux-independent) fixed sink regime. More quantitatively, it suggests that (i) the upper limit to the thermal regime is above 10^{9} n.cm^{-2}s^{-1}, and below 7 × 10^{11} n.cm^{-2}·s^{-1}(ii) the upper limit to the fixed sink regime will be above 7 × 10^{11} n.cm^{-2}s^{-1}. (This places the fixed sink-matrix recombination boundary close to the onset flux for Odette and Mader's UMDs, suggesting that matrix recombination could influence the apparent UMD annealing behaviour.)

In their analysis of SC growth in a number of different steels, Wagner et al. (Wagner et al., 2016) concluded that a fixed sink (flux-independent) regime existed below 1.2 × 10^{12} n.cm^{-2}s^{-1}, with matrix recombination dominant at higher flux. Some authors comparing surveillance and MTR irradiations of Cu-containing steels would agree that there is no effect of flux between 10^{10} and 10^{11} (or even mid-10^{12}) n.cm^{-2} (Hein and May, 2008). Odette and co-workers (Eason et al., 1998), however, identify a finite inverse flux dependence within this range in multiple medium and high-Cu welds and base metals irradiated 0.7–8 × 10^{11} n.cm^{-2}s^{-1} in the IVAR campaign. Some of their data are shown in Figure 7, which illustrates both the consistency of the trend and its magnitude which, once again, is sufficiently small to be indistinguishable from scatter in campaigns with fewer measurements or greater measurement uncertainty.

As with the IVAR low-Cu steels, the hardening of the IVAR high-Cu steels was best described using an effective fluence (p = 0.38 ± 0.12, increasing with increasing Ni and Mn and decreasing

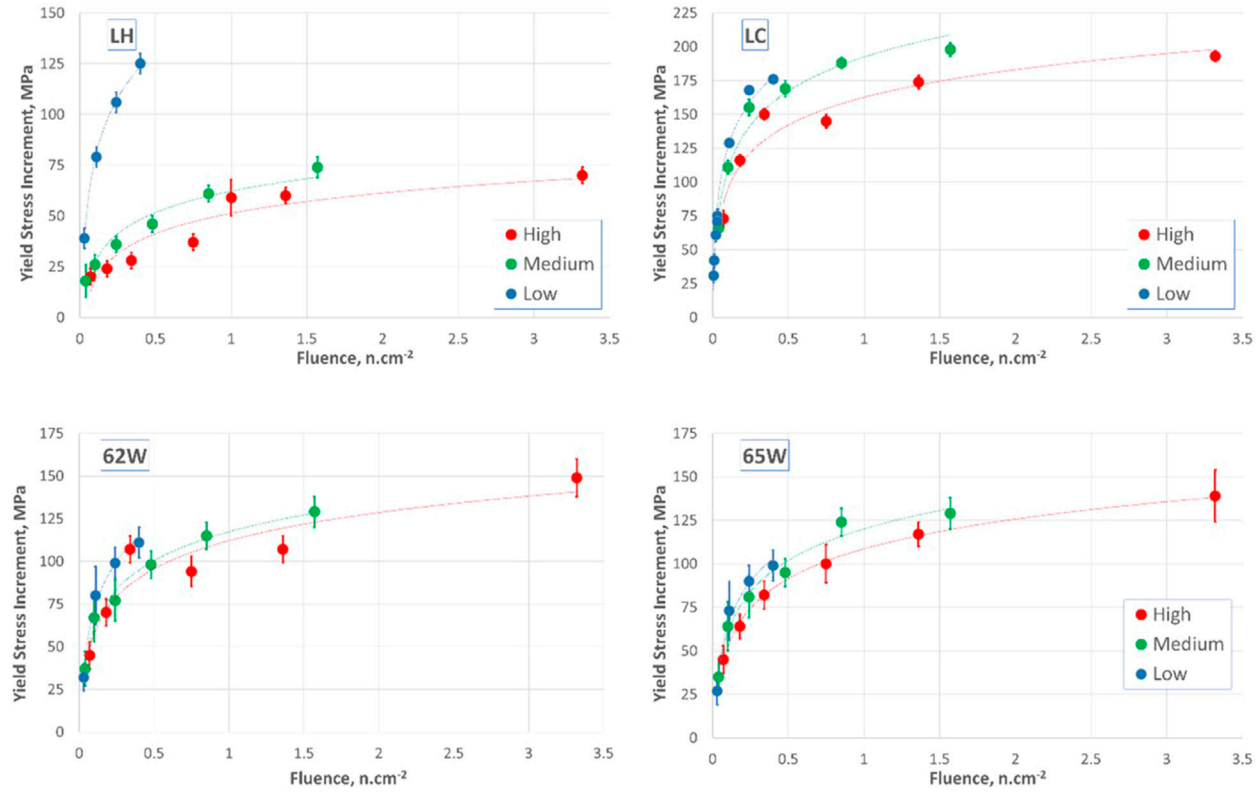

FIGURE 7
Hardening of IVAR high-Cu base metals (LC, LH) and welds (62W, 65 W) at 290°C and high (8–10 × 10^{11} n.cm^{-2}s^{-1}), medium (3 × 10^{11} n.cm^{-2}s^{-1}) and low (8–10 × 10^{10}n.cm^{-2}s^{-1}) fluxes (Data taken from (Eason et al., 2007). LH = 0.11Cu-0.74Ni-1.39Mn-0.005P, LC = 0.41Cu-0.86Ni-1.44Mn-0.005P, 62 W = 0.23Cu-0.60Ni-1.61Mn-0.020P, 64 W = 0.22Cu-0.60Ni-1.45Mn-0.015P. Trend lines are logarithmic best fits to the data.).

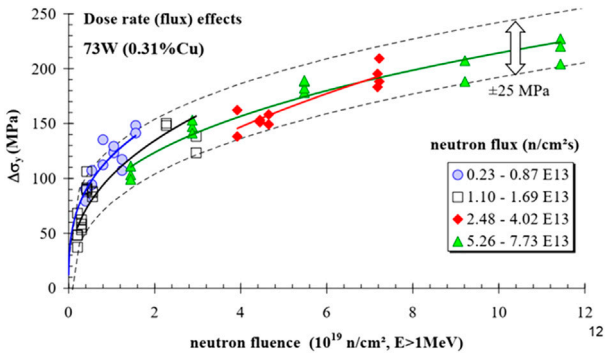

FIGURE 8
Hardening in high-Cu weld at high fluxes (Chaouadi et al., 2008).

Cu) (Eason et al., 1998; Bourgoin et al., 2001; Odette et al., 2001; Odette et al., 2005).

3.2 High fluxes, low fluences (pre-plateau)

Few campaigns obtain much data at fluxes >10^{11} n.cm^{-2} and fluences < 10^{19} n.cm^{-2}.

In their UV-P campaign, Odette, Mader et al. found that increasing the flux from 6 × 10^{11} to 4.6 × 10^{13} n.cm^{-2}s^{-1} decreased the rate of hardening in high-Cu steels. Similarly, Chaouadi et al. observed slight, but consistently decreasing hardening rates with increasing fluxes at low fluences in BR2 irradiations of a 0.31 wt% Cu plate, as illustrated in Figure 8. In consequence of such observations, the RADAMO, ETC contains a flux dependence in the CRP term (although not in the MD term) (Chaouadi et al., 2008). Williams et al. (Williams et al., 1985; Williams et al., 2001b) also saw lower hardening at low-fluences in 0.24–0.56 wt% Cu SAWs irradiated at 2 × 10^{-8} dpa/s versus 6 × 10^{-10} dpa/s(approximately 1.3 × 10^{13} vs. 4 × 10^{11} n.cm^{-2}s^{-1}) with the data converging at higher (plateau) doses. They could not distinguish flux effects in Cu < 0.15 wt % Cu SAWs.

A balance between opposing UMD and CRP responses to increasing flux at fluxes above 10^{12} n.cm^{-2}s^{-1} (plus limited data below 10^{19} n.cm^{-2}) might explain why Hawthorne and Hiser saw higher low-fluence hardening at 6 × 10^{11} n.cm^{-2}s^{-1} than at 9 × 10^{12} n.cm^{-2}s^{-1} in a Linde 80 (0.4 wt% Cu), but not in 0.2 wt% Cu A302B or A533B plates (Hawthorne and Hiser, 1990). The very limited direct support for a UMD effect in studies of low-Cu steels outside UCSB is thus complemented by indirect support from comparative studies of medium-versus high-Cu steels in the UMD range.

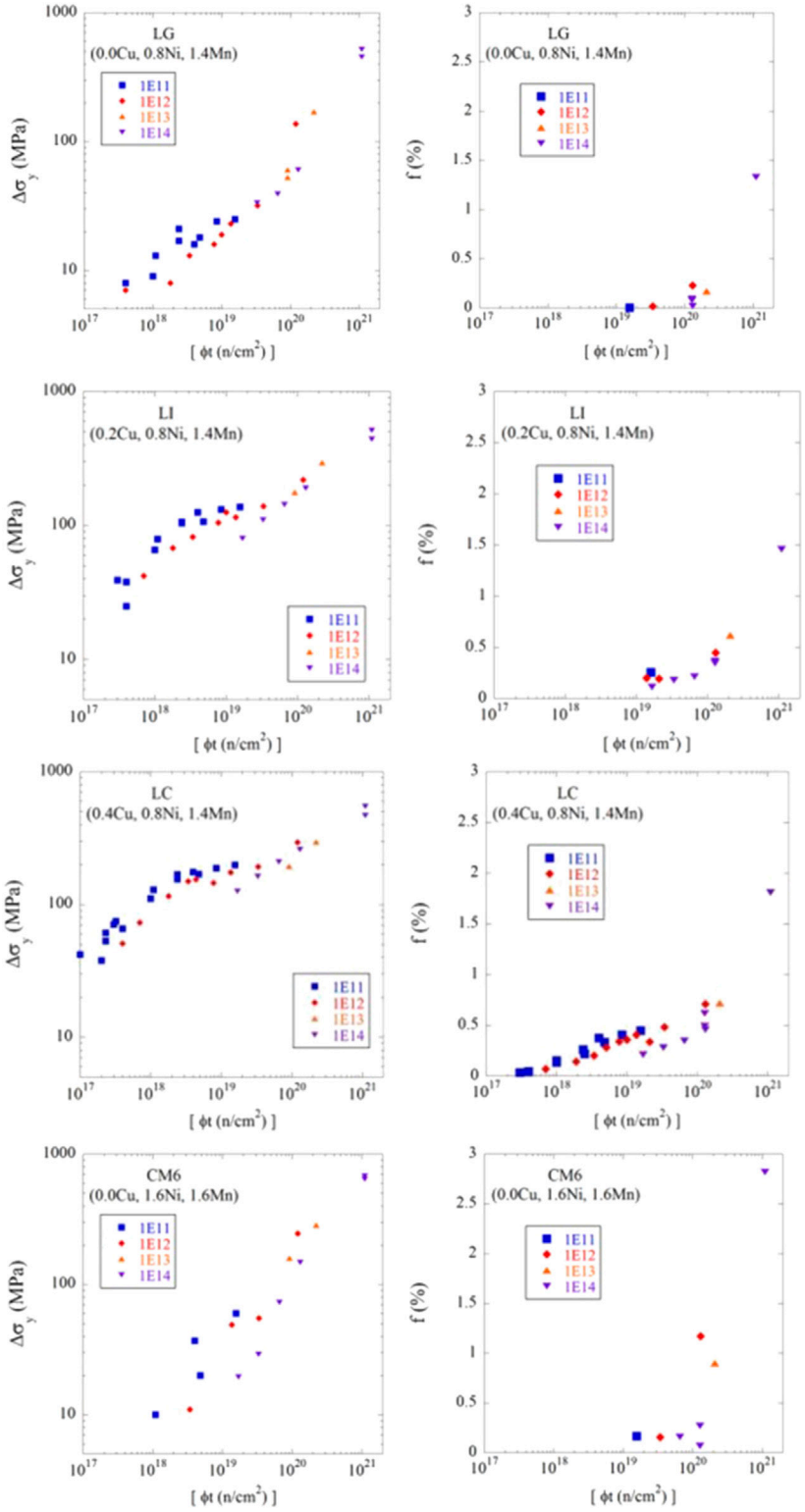

FIGURE 9
Hardening and precipitation in medium -Ni UCSB steels with different Cu and Ni levels (Nanstad et al., 2022).

3.3 Moderate fluences ("on the plateau")

Most authors agree that there is no significant effect of flux on the magnitude of the Cu contribution to hardening or embrittlement once the Cu contribution has reached the plateau. This is found in MTR campaigns at high fluxes (Williams et al., 1985; Langer et al., 2000; Chaouadi et al., 2008) and is also reflected in the forms of the EWO, EONY, ASTM E900-02 and E900-15 embrittlement trend curves derived from US LWR lower-flux surveillance data. Odette et al. (Odette et al., 2005) considered that the plateau level of CRP hardening was generally independent of flux at the low and intermediate dose rates (~8 × 10^{10} n.cm^{-2}s^{-1} and 3 × 10^{11} n.cm^{-2}s^{-1}) but, for some compositions, it was lower at high flux (~8 × 10^{11} n.cm^{-2}s^{-1}).

Microstructurally, increasing the flux tends to produce slightly more, smaller clusters (Williams and Phythian, 1996; Hyde et al., 2001; Dohi et al., 2009; Soneda et al., 2015; Wagner et al., 2016; Hashimoto et al., 2021). Within a classic dispersed barrier model of hardening (DBH), this would be expected to produce a higher plateau in MTR-irradiated materials. In irradiated RPV steels, however, the hardening is more strongly related to $\sqrt{f_v}$ than to $\sqrt{f_v}/r$, (where f_v = volume fraction of SCs and r = SC radius), so the small microstructural change is insufficient to produce a flux-dependence in the plateau which is easily distinguishable from scatter.

3.4 Very high fluences

Even in high-Cu steels, the dissolved Cu is generally reduced to very low levels by 5–10 × 10^{19} n.cm^{-2}. Above this stage, the development of the microstructure is similar in low-and high-Cu steels. In consequence, the flux dependence of hardening and embrittlement follow similar trends.

Once again, much of the systematic data on flux effects comes from UCSB campaigns. Microstructural and hardening data from steels with increasing levels of Cu are shown in Figure 9.

As expected, Figures 9C, E show high initial hardening rate versus fluence (data acquired at 10^{11} and 10^{12} n.cm^{-2}s^{-1}) which diminishes in the range 2–6 × 10^{18} n.cm^{-2} as the Cu precipitation rate diminishes (the onset of the plateau). The data acquired at 10^{12} n.cm^{-2}s^{-1} extend to higher fluences and show an increase in the hardening rate somewhere in the range 6–12 × 10^{19} n.cm^{-2}. The higher rate of hardening is reproduced in the high-fluence data acquired at 10^{13} and 10^{14} n.cm^{-2}s^{-1} although no threshold fluence for a change in hardening rate is evident in these data. In this representation, the 10^{13} and 10^{14} n.cm^{-2}s^{-1} data appear to show a consistent linear hardening rate (on the log-log plot) from low fluences. The hardening and cluster data from 1.6 wt% Ni steels (such as CM6 in Figures 9G, H) also show no change in the rates of increase with fluence but are consistently high.

The UCSB group found that the high-fluence hardening and precipitation data converged when plotted versus the effective fluence with $p = 0.25$, confirming the existence of flux dependence in the regime over which Mn-Ni-Si phases were thought to precipitate. The low derived value of p appears to be due to the density of radiation-induced sinks (solute clusters, dislocation loops, solute-point defect complexes, precipitates) which dominate recombination in contrast to the mutual annihilation of individual point defect anticipated at high flux and low fluences.

In their analysis of the embrittlement data in the PLOTTER database, Kirk and co-workers (Kirk and Erickson, 2021; Kirk and Ferreno Blanco, 2022) were able to reconcile surveillance and MTR data with a trend curve which incorporated a weak negative flux dependence in the term applicable to high-Cu steels, consistent with the UCSB CRP and MNS observations. (The stronger flux effect in high-Cu steels being visible despite the variation in dpa:fluence ratios in the input data.)

3.5 Summary of flux effects in high-Cu steels, knowledge gaps and implication

Hardening and embrittlement in high-Cu steels is greater than in low-Cu steels, making trends easier to observe. In the pre-plateau, low-fluence range:

- The various analyses agree that, in the flux range <~5 × 10^{10} n.cm^{-2}s^{-1}, the embrittlement in Cu-containing steels decreases with increasing flux at a given fluence. The agreement is consistent with understanding that increasing flux will delay the rate at which diffusion-controlled SC growth can occur in the thermal regime, with the thermal regime beginning within the range of fluxes examined in the program. More information is available from high-Cu steels in this flux-fluence regime than was available for the low-Cu steels.
- In the range 5 × 10^{10}–10^{12} n.cm^{-2}s^{-1}, the observations in Cu-containing steels appear split between those who observe no effect of flux within measurement uncertainty and those who observe a decrease in hardening with increasing flux. It is not easy to correlate the alternative observations with fluence range or Cu content. Nonetheless, it is plausible that this is a range of weaker flux-dependence given the data from the low-Cu steels supportive of a fixed sink regime in this flux range.
- At fluxes above 10^{12} n.cm^{-2}s^{-1}, different observations of embrittlement show increases, decreases and no effect with increasing flux. In this flux range, the higher-Cu steels appear more likely to show a decrease and the lower-Cu steels an increase in embrittlement with increasing flux. This is interpretable in terms of a low-fluence UMD effect operating in the opposite sense to a low-fluence, pre-plateau Cu precipitation effect. Alternatively, it could indicate that the effect of flux is monotonic but is more difficult to distinguish from measurement uncertainty at lower fluences and Cu levels.

There is general agreement that hardening in the plateau regime is independent of flux. The importance of diffusion in the development of CRPs allows rate theory models of flux effects on diffusion (e.g. (Williams et al., 2010)) to be applied to mechanical property development in high-Cu as well as low-Cu steels. There are fewer disagreements between campaigns involving higher-Cu steels than were reported for low-Cu steels. This leaves fewer

areas of uncertainty. Further investigation in the 5 × 10^{10}–10^{12} n.cm^{-2}s^{-1} range might help clarify when (or whether) hardening is flux dependent in this range.

Studies on low-Cu steels came to conflicting conclusions concerning the presence of the thermal regime in BWR surveillance data. The direct evidence from the behavior of medium-Cu steels in BWR surveillance irradiations supports the existence for a thermal regime which would affect both low- and high-Cu steels. The overall results indicate that flux effects need to be considered when applying trends derived from surveillance data to the BWR beltline and to "expanded beltline" components during plant life extension periods.

Studies on low-Cu steels were also ambiguous concerning the existence of UMDs (Section 2.3) and the flux-fluence range over which they would have an effect on hardening/embrittlement. The indirect evidence from the difference in the pre-plateau behavior of medium-Cu versus high-Cu steels provides support for the existence of UMDs. The flux-fluence range over which they dominate flux effects remains unclear, affecting the extrapolation of information from high-flux MTR irradiations to beltline conditions in the range 10^{19}–10^{20} n.cm^{-2}s^{-1}.

4 Flux effects on grain boundary segregation and non-hardening embrittlement

MnMoNi steels are not generally prone to intergranular failure, so information on flux effects generally comes from CrMoV steels. Kuleshova et al. (2017) used Auger Electron Spectroscopy (AES) to measure grain boundary segregation in a low-Cu (0.03–0.06 wt%) high-Ni (1.61–1.89 wt%) NiCrMo WWER-1000 Sv-10KhGNMAA weld metal after thermal ageing at 300°C or irradiation in a WWER-1000 surveillance scheme, (8–11 × 10^{10} n.cm^{-2}s^{-1}; E > 0.5 MeV at 300°C to 3 × 10^{19} n.cm^{-2}; E > 0.5 MeV). Some of the thermally-aged samples were subsequently irradiated in a research reactor, IR8 (2–18 × 10^{12} n.cm^{-2}s^{-1}; E > 0.5MeV to 5 × 10^{19} n.cm^{-2}; E > 0.5 MeV). The lower-flux irradiation may be in the thermal or fixed sink regime while the higher fluxes are likely to be in the matrix recombination regime.

In both cases the fluences are high enough that the concentration of radiation-induced sinks is significant: TEM found 3–4 × 10^{21} dislocation loops m^{-3}; APT found 6 × 10^{23} solute clusters m^{-3}. The AES showed that the levels of P, Ni and Cr on the grain boundaries all increased with both thermal ageing and irradiation. The higher-flux irradiation was somewhat less effective at attracting P to the grain boundaries, consistent with the shorter diffusion distances over which complexes drag solutes when matrix recombination (and radiation-induced traps) becomes more important.

No intergranular failure (IGF) was observed in the initial material (14% monolayer P), but increasing amounts were observed with increasing thermal ageing or increasing low-flux irradiation, suggesting a threshold for IGF between 15% and 20% monolayer in these steels.

These observations of P segregation in CrMoV steels suggest that the framework described in the Introduction is relevant, and data from high-flux irradiations will underestimate grain boundary segregation at lower fluxes. Insufficient measurements and modelling exist to quantify this overall trend and show how high flux data should be used to predict P accumulation in RPV grain boundaries even in CrMoV steels.

5 Flux effects at high fluences

5.1 Comparison between high fluence data and threshold/flux models

The most important challenge facing LWR operators looking to extend the reactor lifetime is the possibility of accelerated embrittlement at high fluences due to either the onset of intergranular fracture or the conversion of solute clusters into the nuclei of a distinct phase with a higher hardening capacity. As shown in Section 4, there are insufficient data to quantify the effect of flux on the threshold dose for IGF. It is, however, possible to assess whether an acceleration due to Mn-Ni-Si precipitate formation occurs at fluences above a flux-dependent threshold by comparing the available data with predictions of the RR-UCSB model of flux effects.

The data set with the least ambiguous change in the hardening and solute clustering rate at high fluence is that acquired for medium-Ni steels in the UCSB ATR2 campaign at 10^{12} n.cm^{-2}s^{-1} (red points in Figure 9). For these steels, the hardening data suggest an upswing midway between the two highest-fluence datapoints (3–11 × 10^{19} n.cm^{-2}) while the associated f_v data suggest an upswing closer to the last datapoints. This fluence range does not appear affected by the steels' Cu content. For the high-Ni steels in that program (not included in these Figures), there was no clear upswing in the hardening rate, although the rate was generally high, suggesting a much lower threshold, perhaps as low as the lowest-fluence data point for which hardening was measured at 3 × 10^{18} n.cm^{-2}. The cluster volume fraction measurements suggest a higher fluence for the threshold, perhaps around 1 × 10^{19} n.cm^{-2}.

Taking representative threshold fluences of 8 × 10^{19} n.cm^{-2} for medium-Ni steels and 1 × 10^{19} n.cm^{-2} for high-Ni steels at 10^{12} n.cm^{-2}s^{-1} and 290°C, the fluences required for a similar level of diffusion-controlled microstructural development under different fluxes can be derived using the acceleration factor, Q, developed in the RR-UCSB collaboration (Williams et al., 2010) and given in Figure 4. The equivalent values for the medium-Ni steels are:

- 5.5 × 10^{20} n.cm^{-2} at 10^{14} n.cm^{-2}s^{-1} (Q~0.13)
- 1.8 × 10^{20} n.cm^{-2} at 10^{13} n.cm^{-2}s^{-1} (Q~0.4)
- 8.0 × 10^{19} n.cm^{-2} at 10^{12} n.cm^{-2}s^{-1} (Q~0.9)
- 6.0 × 10^{19} n.cm^{-2} at 10^{11} n.cm^{-2}s^{-1} (Q~1.2)
- 5.5 × 10^{19} n.cm^{-2} at 10^{10} n.cm^{-2}s^{-1} (Q~1.3)
- 5.1 × 10^{19} n.cm^{-2} at 10^{9} n.cm^{-2}s^{-1} (Q~1.4)

These fluences can be compared with the hardening seen in other data sets acquired out to high fluences.

- The predicted threshold for the UCSB ATR data (Odette et al., 2016) acquired at 10^{14} n.cm^{-2}s^{-1} in Figure 9 (mauve points)

TABLE 1 Material compositions and irradiation conditions used in the LONGLIFE program (Altstadt et al., 2014; Hein, 2015).

Material	Type	Composition (wt%)			Flux ($n.cm^{-2}s^{-1}$)	Temp. (°C)	Maximum fluence ($n.cm^{-2}$)	Predicted threshold ($n.cm^{-2}$)	Suggested threshold fluence ($n.cm^{-2}$)
		Cu	Ni	Mn					
EDF1	16MND5 bm	0.09	0.65	1.27	$0.9–2.5 \times 10^{11}$	260	1.2×10^{20}	7×10^{19}	N/S
EDF2	16MND5 bm	0.06	0.69	1.32	2×10^{11}	286	7×10^{19}	6×10^{19}	N/S
EDF3	16MND5 wm	0.03	0.64	1.41	1.5×10^{12}	286	5×10^{19}	6×10^{19}	N/S
RAB1	S3NiMo wm	0.08	1.58	1.46	2×10^{11}	283	5.5×10^{19}	6×10^{19}	N/S
JPB	A533B Cl1 bm	0.01	0.83	1.42	$0.3–9.6 \times 10^{12}$	290	1.6×10^{20}	$7–28 \times 10^{19}$	N/S
JPC	A533B Cl1 bm	0.01	0.81	1.45	$0.3–9.6 \times 10^{12}$	290	1.2×10^{20}	$7–28 \times 10^{19}$	N/S
JPB	A533B Cl1 bm	0.01	0.83	1.42	$0.1–3.5 \times 10^{12}$	255*	9×10^{19}	1.2×10^{20}	$6–9 \times 10^{19}$
JPC	A533B Cl1 bm	0.01	0.81	1.45	$0.1–3.5 \times 10^{12}$	255*	9×10^{19}	1.2×10^{20}	$6–9 \times 10^{19}$

N/S no threshold seen, bm, base metal; wm, weld metal. * Only 3 points shown on plot.

lies between the two highest-fluence data points. The $\Delta\sigma_Y$ and f_v values for steel LG are consistent with the prediction, although the increase in the rate of hardening is not very strong on the log-log scale. The f_v values for the higher-Cu steels LI and LC also support this analysis, although the $\Delta\sigma_Y$ data do not: no increase in hardening rate is evident between the last two data points for these steels. Overall, the data are weakly supportive of the prediction.

- All the UCSB data acquired at 10^{13} $n.cm^{-2}s^{-1}$ in Figure 9 (orange points) lie above the threshold, so no change in hardening or precipitation rate need be evident in the data. In accordance with this, no change in hardening rate is evident in the data for any of the steels, while the f_v levels are similar to those seen in the post-threshold 10^{12} $n.cm^{-2}s^{-1}$ data. Again, the data are weakly supportive.
- The UCSB data acquired at 10^{11} $n.cm^{-2}s^{-1}$ in Figure 9 (blue points) are all below the threshold, so all the hardening should be at the lower rate, and no additional f_v should be evident. This is in accordance with the observed $\Delta\sigma_Y$ and f_v data. Such data cannot really be considered to support or contradict the analysis.
- The Belgian data reaching to the highest fluences in Figure 8 were acquired at $5.2–7.7 \times 10^{13}$ $n.cm^{-2}s^{-1}$ and 300°C (Q~0.15) so the threshold is predicted to be around 4.8×10^{20} $n.cm^{-2}$. The data in Figure 8 have been used to suggest that there is no late-onset increase in the rate of embrittlement, but with a maximum fluence around 1.17×10^{20} $n.cm^{-2}$, all the data are predicted to lie below the threshold. The monotonic trend curve in the Figure thus neither does supports nor contradicts the analysis.
- The Rolls-Royce low-Ni SAW data in Figure 3 (Williams et al., 2001a; Williams et al., 2001b) showed no high-dose upswing out to 32mdpa (~2.2×10^{19} $n.cm^{-2}$) at 255°C and 7×10^{-9} dpa/s (about 4.7×10^{12} $n.cm^{-2}s^{-1}$). Given the relatively low dose, it is not surprising that the measurements are also all predicted to be below the threshold.

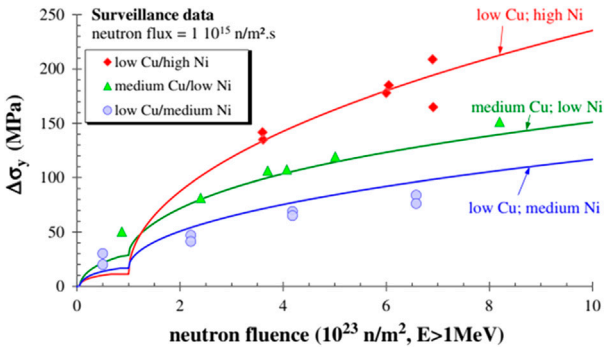

FIGURE 10
Comparison between RADAMO predictions and hardening of a number of steels in the SCK.CEN database (Chaouadi and Gerard, 2013)[2].

- Analysis of the Rolls-Royce high-Ni SAW data is a little more complex, but more consistent with a threshold of 3×10^{18} $n.cm^{-2}s^{-1}$ than 1×10^{19} $n.cm^{-2}$. With the lower threshold, the RR high-Ni SAW data at 4×10^{-8} dpa/s (crosses) are above the threshold and the data at 7×10^{-9} dpa/s (open squares) cross the threshold. The location of the lower-dose 7×10^{-9} dpa/s data, above the trend line drawn in the Figure, is consistent with a change in hardening rate at the required dose (as well as with measurement uncertainty, as assumed in the plot). The 7×10^{-10} dpa/s data (triangles) should also cross the threshold, but the lower-dose data are sufficiently close to the threshold that this might be difficult to observe. Similarly, the 9×10^{-11} dpa/s data (circles) should lie below the threshold, but the absolute hardening is so small at the low doses involved that comparison with the higher-dose rate data is difficult. Overall, the RR high-Ni data are consistent with the existence of a threshold in high-Ni steels, if not strongly so. The threshold is sufficiently low

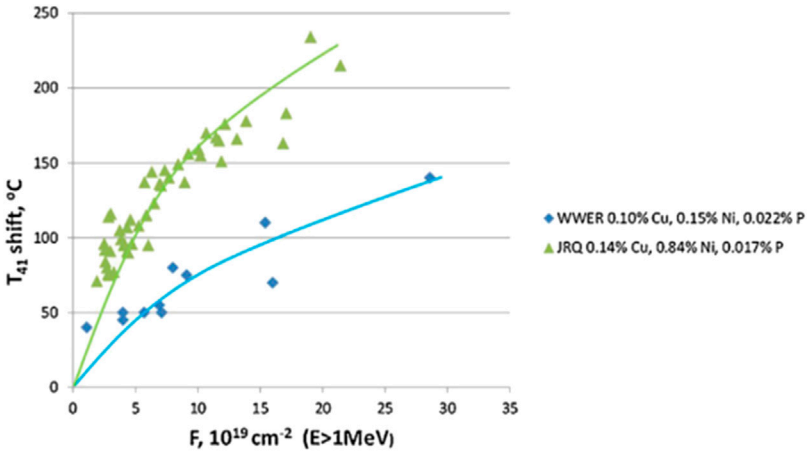

FIGURE 11
High fluence data from 15Kh2MFA CrMoV WWER steel and A533B plate (JRQ) irradiated at 270°C and fluxes between 1011 and 1012 n.cm^{-2}s^{-1} (Castin et al., 2022)[3].

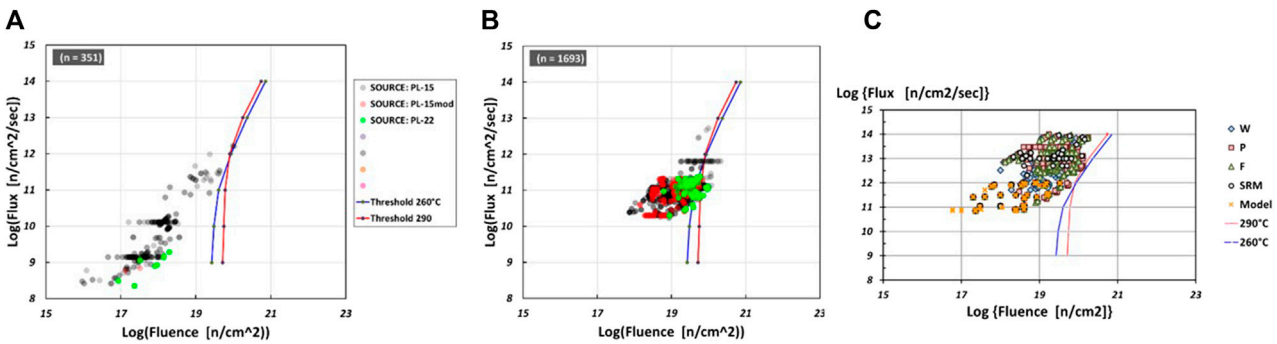

FIGURE 12
Comparison between data in ASTM PLOTTER database and predicted threshold **(A)** BWR surveillance data **(B)** PWR surveillance data **(C)** MTR data. (Blue diamonds = welds, orange squares = plates, green triangles = forgings, open circles = standard reference materials, yellow crosses = model alloys, red line = threshold at 290°C, blue line = threshold at 260°C).

that high embrittlement rates will be expected in high-Ni RPV components from early in life, so no further acceleration is likely to be introduced by long term operation.

- The Euratom-funded LONGLIFE program was set up to collate data from a range of commercial steels irradiated to high fluences (Altstadt et al., 2014; Hein, 2015). The results are summarized in Table 1. In two cases, a high-fluence acceleration in hardening was identified in the data but at a fluence well below prediction. With only three datapoints in each set, however, it was difficult to confirm that a change in hardening rate had, indeed occurred. In five cases, no acceleration was observed and the highest fluence was predicted to be at or below the threshold. These data can neither confirm nor contradict the model. In only one case (EDF-1) were multiple data points acquired both before and significantly beyond the predicted threshold fluence, without an acceleration being identified, contradicting the model.
- Figure 10 shows surveillance data from within the RADAMO database acquired at fluxes around 10^{11} n.cm^{-2}s^{-1} (Chaouadi and Gerard, 2011). The Q-factor analysis suggests that a change in the fluence-dependence of hardening should occur around 6×10^{19} n.cm^{-2}s^{-1} for the medium-Ni steel, and at a higher fluence for a low-Ni steel, making all these data pre-threshold. The absence of acceleration in the low- and medium-Ni data sets is consistent with the proposition, but does not confirm it. The predicted threshold for a high-Ni steel would be between 2–8 $\times$ 10^{18} n.cm^{-2} (depending on the definition of the CM6 threshold), such that all the high-Ni data would be post-threshold. The higher hardening rate with respect to the lower-Ni steels and the absence of acceleration in the high-Ni data set is also consistent with the proposition.
- Figure 11 shows embrittlement data from the IAEA reference steel JRQ acquired at 270°C and fluxes between 10^{11}–10^{12} n.cm^{-2}s^{-1}. Again, the lower-fluence data were

likely to have been acquired at lower fluxes. With Q values between 0.9 and 1.2, this puts the threshold around 7×10^{19} n.cm^{-2}. This is a valuable data set in that it contains a large number of measurements out to high fluences. A monotonic trend line is drawn through the data, although a better fit might be achieved with either (i) a steeper early curve and shallower later curve, or (ii) a more sharply bending curve at lower fluences, plus a threshold to a higher hardening rate above about 1.7×10^{20} n.cm^{-2}. If the last two data points in Figure 11 are truly above a threshold, rather than exhibiting scatter, however, this threshold occurs at more than twice the predicted fluence.

Figure 12 compares the predicted threshold fluence values at 260°C and 290°C and different fluxes with the fluxes and fluences of data in the ASTM PLOTTER database. The predicted thresholds are above all the BWR surveillance data (as of 2022), but 5%–10% of the PWR data are above the predicted thresholds at 290°C. The MTR data (as of 2015) are also below the predicted thresholds. Given the uncertainties in the calculations, it is unlikely that any late-onset increase in the embrittlement rate will be evident in the surveillance data. In consequence current embrittlement trend curves will not incorporate any influence from the predicted acceleration. (The absence of a high-fluence increase in the embrittlement rate within the PLOTTER data is also supported by the multiscale modelling shown in (Castin et al., 2022) which successfully predicts the behaviour of the low-Cu steels within PLOTTER via a model which does not allow for precipitation.)

- Nine low- and medium-Ni commercial steels irradiated in surveillance programs (exposures in the range 7×10^{18} ~9×10^{19} n.cm^{-2} at 0.9–1.6 × 10^{11} n.cm^{-2}s^{-1}) were re-irradiated in an MTR in the UCSB ATR-2 campaign (to ~1.4×10^{20} n.cm^{-2} at 3.6×10^{12} n.cm^{-2}s^{-1} (Q~0.65) At the surveillance fluxes (Q~1.2), the threshold fluence would convert to around 6×10^{19} n.cm^{-2}, so surveillance points would lie below and above the threshold. Around half of the eight steels can be described as showing an acceleration in hardening, generally between the surveillance and MTR points. Given the scatter in the surveillance measurements, the uncertainty in the threshold value and the small number of points likely to be above the threshold, this comparison does provide clear confirmation of the threshold model, but does not contradict it.

In summary, few of the data sets extending to high fluences exhibit a late onset acceleration in hardening/precipitation rates. In the majority of cases, the Q-based analysis suggests that this is because the data all fall above or below a flux-dependent threshold. These campaigns cannot help determine whether or not late-onset acceleration occurs. In only one of the data sets is a threshold predicted to be present (on the basis of the UCSB data acquired at 10^{12} n.cm^{-2}s^{-1} (Odette et al., 2016) and the Q analysis) plausibly observed (irradiations at 10^{14} n.cm^{-2}s^{-1} in (Odette et al., 2016)). In several others, a predicted threshold may or may not be present given the scatter in the data. In two data sets with multiple measurements each side of the predicted threshold, however, no acceleration is seen (EDF-1 (Altstadt et al., 2014; Hein, 2015) and JRQ (Kryukov et al., 2014)). At best, this constitutes only weak support for a late-onset threshold. Nonetheless, because the UCSB data acquired at 10^{12} n.cm^{-2}s^{-1}, plus the RR-UCSB description of flux dependences, lead to a prediction that PWR designs with beltline fluxes around 10^{11} n.cm^{-2}s^{-1} will exceed the threshold in long term operation, it is important to provide clearer confirmation/rejection of the flux-dependent threshold hypothesis. The threshold values listed for different fluxes in this Section provide useful input into the design of appropriate experiments.

6 Summary and conclusion

A framework in which to understand flux effects was suggested in the 1970s. It postulates a thermal region at low fluxes, and intermediate fixed sink regime and a high flux matrix recombination regime. This review has shown that the framework remains useful, identifies ranges for some of the regimes, and recognises that fixed sink regime expands with increasing fluence.

Flux effects in low-Cu steels are more difficult to distinguish from measurement uncertainty, but comparisons between low- and high-Cu steels suggest that flux dependences are present in both composition categories. With different flux-dependences in different regimes, monotonic extrapolation from MTR to surveillance or vessel fluxes is inappropriate in high-Cu steels and would be associated with significant uncertainty in low-Cu steels. The conditions under which unstable matrix defects may be found, and the extent to which they affect hardening, remain unclear. Suggestions have been made for clarifying experiments.

An acceleration in embrittlement at high fluences has been predicted for some years based on the radiation-induced segregation of grain boundary P and consequent introduction of intergranular fracture, but insufficient data exist to identify whether such a threshold occurs under the flux-fluence conditions of long-term operation. This question requires further investigation. A series of campaigns by a well-respected group at UCSB has identified a threshold for accelerated embrittlement at high fluences due to precipitation. An associated model, describing the accelerating effects of flux on precipitation, leads to the conclusion that acceleration will be observed in some PWR RPVs during very long-term operation. The predictions are not, however, well-supported by appropriate data from other sources and, in some cases, are clearly contradicted. Although it can be difficult to obtain funding for "repeat experiments", the technological importance of the issue requires that further observations in flux-fluence ranges encompassing predicted thresholds be performed.

Author contributions

SO: Conceptualization, Writing–original draft. PS: Writing–review and editing. EL: Conceptualization, Project administration, Writing–review and editing.

Funding

The author(s) declare financial support was received for the research, authorship, and/or publication of this article. The authors are grateful to EPRI for the provision of funding to perform this review under Source Agreement MA 10013253 and to NNL for the provision of additional funds for preparation of the paper under Order 30031.221.

Acknowledgments

The authors wish to thank fellow members of EPRI and the UK's Radiation Embrittlement Forum for helpful discussions and insights on the subject of this paper.

Conflict of interest

The authors declare that the research was conducted in the absence of any commercial or financial relationships that could be construed as a potential conflict of interest.

Publisher's note

All claims expressed in this article are solely those of the authors and do not necessarily represent those of their affiliated organizations, or those of the publisher, the editors and the reviewers. Any product that may be evaluated in this article, or claim that may be made by its manufacturer, is not guaranteed or endorsed by the publisher.

References

Altstadt, E., Keim, E., Hein, H., Serrano, M., Bergner, F., Viehrig, H.-W., et al. (2014). FP7 Project LONGLIFE: overview of results and implications. *Nucl. Eng. Des.* 278, 753–757. doi:10.1016/j.nucengdes.2014.09.003

ASTM (2015). *ASTM E900-15. Standard guide for predicting radiation-induced transition temperature shifts in reactor vessel materials*. Pennsylvania, United States: ASTM. April.

Becquart, C. S., and Wirth, B. D. (2020). "Kinetic monte CarloSimulations of irradiation effects chapter 1.14," in *Comprehensive nuclear materials*, 393–410.

Bourgoin, J., Rupa, N., Bache, A., Buisine, D., Rouillon, Y., and Bezdekian, G. (2001). "The pressure vessel surveillance program of the French PWRs," in Proc. Workshop on Dose Rate Effects in Reactor Pressure Vesel Materials, Squaw Valley, CA, USA, November 2001.

Brillaud, C., and Hedin, F. (1992). "In-service evaluation of French pressurised water reactor vessel steel," in *Effects of radiation on materials: 15th int. Symp. ASTM STP 1125* (ASTM), 23–49.

Burke, M. G., Stofanak, R. J., Hyde, J. M., English, C. A., and Server, W. L. (2003). "Microstructural aspects of irraiation damage in A508 Gr 4N forging steel: composition and flux effects," in Effects of Radiation on Materials: 21st Int. Symp. ASTM STP 1447, West Conshohocken, PA, USA, January 2003.

Castin, N., Bonny, G., Bakaev, A., Bergner, F., Domain, C., Hyde, J., et al. (2020). The dominant mechanisms for the formation of solute-rich clusters in low-Cu steels under irradiation. *Mater. Today Energy* 17, 100472. doi:10.1016/j.mtener.2020.100472

Castin, N., Bonny, G., Konstantinovic, M. J., Bakaev, A., Bergner, F., Courilleau, C., et al. (2022). Multiscale modelling in nuclear ferritic steels: from nano-sized defects to embrittlement. arXiv preprint, arXiv2204.11441 Available at: https://arxiv.org/abs/2204.11441.

Castin, N., Malerba, L., and Chaouadi, R. (2011). Prediction of radiation induced hardening of reactor pressure vessel steels using artificial neural networks. *J. Nucl. Mater.* 408, 30–39. doi:10.1016/j.jnucmat.2010.10.039

Chaouadi, R., and Gerard, R. (2011). Neutron flux and annealing effects on irradiation hardening of RPV materials. *J. Nucl. Mater.* 418, 137–142. doi:10.1016/j.jnucmat.2011.06.012

Chaouadi, R., and Gerard, R. (2013). Confirmatory investigations on the flux effect and associated unstable matrix damage in RPV materials exposed to high neutron fluence. *J. Nucl. Mater.* 437, 267–274. doi:10.1016/j.jnucmat.2013.02.029

Chaouadi, R. (2005). *An engineering radiation hardening model for RPV materials. SCK.CEN Report R-4235*. Belgium: SCK.CEN, Mol.

Chaouadi, R., van Walle, E., and Gerard, R. (2008). "The RADAMO experimental program in support of the RPV radiation hardening modeling activities at SCK.CEN," in Workshop on Trend Curve Development for Surveillance Data with Insight on Flux Effects at High Fluence: Damage Mechanisms and Modeling, Mol, Belgium, November 2008.

Dohi, K., Nishida, K., Nomoto, A., Soneda, N., Matsuzawa, H., and Tomimatsu, M. (2009). "Effect of additional irradiation at different fluxes on RPV embrittlement PVP2009-77658," in Proc ASME Pressure Vessels And Piping Division Conference, PVP2009, Prague, Czech Republic, July, 2009.

Dohi, K., Soneda, N., Onchi, T., Ishino, S., Odette, G. R., and Lucas, G. E. (2001). "Dose rate effect in low copper steels irradiated in FNR," in Proc. Workshop on Dose Rate Effects in Reactor Pressure Vessel Materials, Squaw Valley, CA, USA, November 2001.

Eason, E. D., Odette, G. R., Nanstad, R. K., and Yamamoto, T. (2007). *A physically based correlation of irradiation-induced transition temperature shifts. ORNL/TM-2006/530*. Oak Ridge, Tennessee: Oak Ridge National Laboratory.

Eason, E. D., Wright, J. E., and Odette, G. R. (1998). *Improved embrittlement correlations for reactor presure vessel steels. NUREG/CR-6551*. Wahsington DC, USA: US Nuclear Regulatory Commission. November.

EPRI (2009). *BWR reactor pressure vessel embrittlement correlation studies. BWRVIP-216NP: BWR Vessels and internals project*. Palo Alto, CA, USA: EPRI.

Gerard, R., Lucon, E., Scibetta, M., Chaouai, R., and Van Walle, E. (2006). "Reactor pressure vessel steels embrittlement at very high neutron doses," in 6th Int. Conf. On Contribution Of Materials Investigtions To Improve The Safety And Performance Of LWRs: Fontevraud VI, Avignon, France, September 2006.

Hashimoto, Y., Nomoto, A., Kirk, M., and Nishida, K. (2021). Development of new embrittlement trend curve based on Japanese surveillance and atom probe tomography data. *J. Nucl. Mater.* 553, 153007. doi:10.1016/j.jnucmat.2021.153007

Hawthorne, J. R., and Hiser, A. L. (1990). *Influence of fluence rate on radiation-induced mechanical property changes in RPV steel NUREG/CR 5493*. Washington, DC, United States: US Nuclear Regulatory Commission.

Hein, H. (2015). "Position paper on RPV radiation embrittlement issues based on the outcome of the Euratom FP7 project LONGLIFE," in *Trans. SMiRT-23* (Manchester, UK).

Hein, H., and May, J. (2008). "Review of irradiation surveillance and test reactor data of RPV steels used in German LWR in relation to the flux effect issue," in Workshop on Trend Curve Development with insight on Flux Effects at High Fluence: Damage Mechanisms and Modeling, Mol, Belgium, November 2008.

Hyde, J. M., Ellis, D. E., English, C. A., and Williams, T. J. (2001). "Microstructural evolution in high-Ni submerged arc welds," in *Effects of radiation on materials: 20th int. Symp. ASTM STP 1405*.

Japan Nuclear Energy Safety Organisation (2009). *Report on radiation embrittlement at high fluences. 08 base metal report-0005*. January.

Kirk, M., and Erickson, M. (2021). *Methods to address the effects of irradiation embrittlement in section XI of the ASME code estimation of an irradiated reference temperature using either traditional Charpy approaches or master curve data. 3002020911*. Palo Alto, CA, USA: EPRI.

Kirk, M., and Ferreno Blanco, D., (2022) "Evaluation of the ASTM E900-15 DT41J prediction equation in light of new data," in ASTM Symposium on Trend Curve Development, Prague, Czech Republic, April 2022.

Kryukov, A., Nanstad, R. K., and Brumovsky, M. (2014). Common comparison of the irradiation embrittlement of WWER/PWR reactor pressure vessel steels. *Nucl. Eng. Des.* 273, 175–180. doi:10.1016/j.nucengdes.2014.03.018

Kuleshova, E. A., Gurovich, B. A., Lavrukhina, Z. V., Maltsev, D. A., Fedotova, S. V., Frolov, A. S., et al. (2017). Study of the flux effect nature for VVER-1000 RPV welds with high nickel content. *J. Nucl. Mater.* 483, 1–12. doi:10.1016/j.jnucmat.2016.10.030

Langer, R., Bartsch, R., and Foehl, J. (2001). "Irradiation results for different reactors," in Proc Workshop on Dose Rate Effects in Reactor Pressure Vessel Materials, Squaw Valley, CA, USA, November 2001.

Langer, R., Bartsch, R., and Nagel, G. (2000). "Irradiation behavior of submerged arc welding materials with different copper contents," in *Effects of radiation on materials: 19th int. Symp. ASTM STP 1366* (West Conshohocken, PA, Unites States: ASTM), 235–244.

Lindgren, K., Boasen, M., Stiller, K., Efsing, P., and Thuvander, M. (2017). Evolution of precipitation in reactor pressure vessel steel welds under neutron irradiation. *J. Nucl. Mater.* 488, 222–230. doi:10.1016/j.jnucmat.2017.03.019

Mader, E. V. (1995). *Kinetics of irradiation embrittlement and the post-irradiation annealing of nuclear reactor pressure vessel steels: D. Phil dissertation. UMI No. 9617674*. Santa Barbara, CA, USA: Deaprtment of Materials Engineering, University of California. August.

Mathew, J., Parfitt, D., Wilford, K., Riddle, N., Alamaniotis, M., Chroneos, A., et al. (2018). Reactor pressure vessel embrittlement: insights from neural network modelling. *J. Nucl. Mater.* 502, 311–322. doi:10.1016/j.jnucmat.2018.02.027

Nanstad, R., Almirall, N., Server, W., Wells, O., Sokolov, M., Long, E., et al. (2022). "On high fluence irradiation hardening of nine RPV surveillance steels in the UCSB ATR-2 experiment: implications to extended life embrittlement predictions," in ASTM Symposium on Trend Curve Development, Prague, Czech Republic, April 2022.

Odette, G. R., and Lucas, G. E. (1998). Recent progress in understanding reactor pressure vessel steel embrittlement. *Radiat. Eff. Defects Solids* 144, 189–231. doi:10.1080/10420159808229676

Odette, G. R., Lucas, G. E., and Klingensmith, D. (2001). "Recent data and analysis on flux effects on RPV embrittlement," in Proc. Workshop on Dose Rate Effects in Reactor Pressure Vessel Materials, Squaw Creek, CA, USA, November 2001.

Odette, G. R., Mader, E. V., Lucas, G. E., Phythian, W. J., and English, C. A. (1993). "The effect of flux on the irradiation hardening of pressure vessel steels," in *Effect of radiation on materials: 16th int. Symp. ASTM STP 1175* (Philadelphia, PA, USA: ASTM), 373–393.

Odette, G. R., Yamamoto, T., and Klingensmith, D. (2005). On the effect of dose rate on irradiation hardening of RPV steels. *Philos. Mag.* 85 (4-7), 779–797. doi:10.1080/14786430412331319910

Odette, G. R., Yamamoto, T., Wells, P. B., and Almirall, N. (2016). *High fluency low flux embrittlement models of LWR reactor pressure vessel embrittlement and a supporting database from the UCSB ATR-2irradiation experiment. Final Report Project No. 11-3176*. Santa Barbara, CA, Unites States: US DOE Nuclear Energy University Program. January.

Petrequin, P. (1996). "IAEA Report IWG-LMNPP-95/5-Vol.1 Proc Specialists meeting on irradiation embrittlement and mitigation," in Proc Specialists meeting on irradiation embrittlement and mitigation, Espoo, Finland, October 23–26, 1995. Vienna, Austria: International Atomic Energy Agency, 95–147.

Server, W., English, C. A., Naiman, D., and Rosinski, S. (2001). *Charpy embrittlement correlations - status of combined mechanistic and statistical bases for US RPV steels: PWR Materials Reliability Program (PWRMRP) EPRI Report 1000705*. Palo Alto, CA, USA: EPRI.

Sizmann, R. (1978). The effect of radiation upon diffusion in metals. *J. Nucl. Mater.* 69-70, 386–412. doi:10.1016/0022-3115(78)90256-8

Soneda, N. (2007). "Multiscale computer simulations and predictive modeling of RPV embrittlement," in *MATGEN-IV, cargese, corsica, France*. September.

Soneda, N. (2010). "Current understanding on the mechanism of neutron irradiation embrittlement," in USNRC Speonsored Workshop on Development of Predictive Models Of Neutron Irradiation Embrittlement In Reactor Pressure Vessel Steels To Support Worldwide Efforts On Nuclear Power Plant Life Extension, Rockville, USA, September 2010.

Soneda, N., Dohi, K., Nishida, K., Nomoto, A., and Matsuzawa, H. (2008). "Effect of fluence and flux on the embrittlement of highly irradiated RPV steels," in Workshop on Trend Curve Development, Mol, Belgium, November 2008.

Soneda, N., Dohi, K., Nishida, K., Nomoto, A., Tomimatsu, M., Matsuzawa, H., et al. (2009). Microstructural characterization of RPV materials irradiated to high fluences at high flux. *J. ASTM Intl* 6 (7), 102128. doi:10.1520/jai102128

Soneda, N., Nishida, K., Nomoto, A., and Dohi, K. (2015). "Flux effect on embrittlement of reactor pressure vessel steels irradiated to high fluences," in Fontevraud 8: International Symposium on Contribution of Materials Investigations and Operating Experience to LWRs' Safety, Performance and Reliability, Avignon, France, April, 2015.

Soneda, N., and Nomoto, A. (2008). "Characteristics of the new embrittlement correlation method for the Japanese reactor pressure vessel steels," in Proceedings of the 17th International Conference on Nuclear Engineering, ICONE17-75320, Brussels, Belgium, May 11-15, 2008.

Stoller, R. E. (2003). "The effect of neutron flux on radiation-induced embrittlement in reactor pressure vessel steels," in *Effects of radiation on materials: 21st int. Symp. ASTM STP 1447*. Editors M. L. Grossbeck, T. R. Allen, R. G. Lott, and A. S. Kumar (West Conshohocken, PA, USA: ASTM), 326–337.

Stoller, R. E. (2020). "Primary radiation damage formation chapter 1.11," in *Comprehensive nuclear materials*, 293–332.

Tomimatsu, M., Urabe, Y., Sanoh, J., Iida, M., Nakamura, T., and Tamura, A. (1994). "Evaluation of RPV steel surveillance programme in Japanese PWR: radiation embrittlement predictions," in Proceedings of the 3rd International Symposium on Contribution of Materials Investigation to the Resolution of Problems Encountered in Pressurized Water Reactors, Fontevraud, France, May 1994.

Toyama, T., Yamamoto, T., Ebisawa, N., Inoue, K., Nagai, Y., and Odette, G. R. (2020). Effects of neutron flux on irradiation-induced hardening and defects in RPV steels studied by positron annihilation spectroscopy. *J. Nucl. Mater.* 532, 152041. doi:10.1016/j.jnucmat.2020.152041

Wagner, A., Bergner, F., Chaouadi, R., Hein, H., Hernandez-Mayoral, M., Serrano, M., et al. (2016). Effect of neutron flux on the characteristics of irradiation-induced nanofeatures and hardening in pressure vessel steels. *Acta mater.* 104, 131–142. doi:10.1016/j.actamat.2015.11.027

Williams, T., Wilford, K., Odette, G. R., and Yamamoto, T. (2010). "A new model of irradiation hardening in low copper RPV steels from stable matrix damage," in Proc IAEA Technical Meeting on Irradiation Embrittlement and Life Management of Reactor Pressure Vessels in Nuclear Power Plant, Znojmo, Czech Republic, October 2010.

Williams, T. J., and Ellis, D. (2001). "A mechanistically-based model of irradiation damage in low alloy steel sumberged arc welds," in *Effects of radiation on materials: 20th int. Symp. ASTM STP 1405* (West Conshohocken, PA, United States: ASTM), 8–27.

Williams, T. J., Ellis, D., English, C. A., and Hyde, J. (2001a). "A model of irradiation damage in high nickel submerged arc welds," in IAEA/LMNPP Specialists Meeting On Irradiation Embrittlement And Mitigation, Gloucester, UK, May 2001.

Williams, T. J., Ellis, D., and O'Connell, W. (2001b). "Dose rate effects in high and low nickel welds," in Proc. Workshop on Dose Rate Effects in Reactor Pressure Vessel Materials, Squaw Valley, CA, USA, November 2001.

Williams, T. J., Ellis, D., Swan, D. I., McGuire, J., Walley, S. P., English, C. A., et al. (1985). "The influence of copper, nickel and irradiation temperature on the irradiation shift of low alloy steels," in Proc. 2nd ANS Int. Symp. Environmental Degradation of Materials in Nuclear Power Systems - Water Reactors, Monterey, California, USA, September 1985.

Williams, T. J., and Phythian, W. J. (1996). "Electron microscopy and small angle neutron scattering study of precipitation in low alloy steel submerged arc welds," in *Effects of radiation on materials: 17th int. Symp. ASTM STP 1270* (Philadelphia, USA).

Xu, Y., Jia, X., Zhang, C., Ning, G., and Yu, Q. (2000). "The effects of flux on radiation embrittlement of low-copper pressure vessel steels," in Effects of Radiation on Materials: 16th Int. Symp. ASTM STP 1366, West Conshohocken, PA, USA, January 2000 (West Conshohocken, PA, United States: ASTM), 118–126.

Yamamoto, T., Matsui, H., Narui, M., and Dohi, K. (2001). "Flux effects on the subsize Charpy impact properties of neutron irradiated A533B steel," in Proc. Workshop on Dose Rate Effects in Reactor Pressure Vessel Materials, Squaw Creek, CA, USA, November 2001.

Nomenclature

ASTM	American Society for Testing and Materials
ATR	Advanced Test Reactor (MTR in US)
BR2	MTR in Belgium
BWR	Boiling water reactor
CRP	Copper-rich SC
Cm	centimetre
dpa	Displacement per atom
ETC	Embrittlement trend curve
FIM, FIS	French median and upper bound embrittlement trend curves
IAEA	International Atomic Energy Agency
IVAR	Irradiation Variables (radiation campaign)
JEAC	Japan Electrical Association Code
LWR	Light water reactor
MD	Matrix defect
MF	Matrix feature
MNS	SC or precipitate containing mainly manganese, nickel and silicon
MTR	Materials test reactor
N	Neutron
PIA	Post-irradiation annealing
ps	Picosecond
PWR	Pressurised water reactor
Q	Hardening acceleration factor
RADAMO	Belgian embrittlement trend curve
RPV	Reactor pressure vessel
RR	Rolls-Royce
S	Second
SAW	Submerged arc weld
SC	Solute cluster
SCK.CEN	Studiecentrum voor de Toepassingen van de Kernenergie. Centre d'Etude de L'Energie Nucleaire (Belgian Nuclear research centre)
SIA	Self-interstitial atom
SMD, SMF	Stable matrix damage/defect, stable matrix feature
T	Time
UCSB	University of California at Santa Barbara
UMD, UMF	Unstable matrix damage/defect, unstable matrix feature
US	United States of America
UV-P	Irradiation campaign carried out in the University of Virginia and Pluto MTRs

ϕ	Flux
ϕt	Fluence
ϕt_e	Effective (flux-compensated) fluence